FINAL TECHNICAL REPORT

i. ADMINISTRATIVE:

Recipient: University of Hawaiʻi at Mānoa

Principal Investigator: Thomas Giambelluca

Project Title: Cloud Water Interception in Hawaiʻi: Developing Capacity to Characterize the Spatial Patterns and Effects on Water and Ecological Processes responses in Hawaiʻi

Report Authors: Han Tseng, Lucas Berio Fortini, Alan Mair, Aurora Kagawa-Viviani, Stephanie Yelenik, Yoshiyuki Miyazawa, Michael Nullet, Joseph Kennedy, John DeLay, Christina Leopold, and Thomas Giambelluca

Award Number: G15AC00159

Report Date: 03/01/2021

Performance Period: 9/1/2015 – 8/31/2020

Award Amount: $458,861

ii. PUBLIC SUMMARY:

Cloud-water interception (CWI) is the process by which fog or cloud water droplets are captured and accumulate on the leaves and branches of plants, some of which drips to the ground. Prior studies in Hawai'i indicate that CWI is highly variable and can contribute substantially to total precipitation. In this study, we monitored CWI and other processes at five mountain field sites on the Islands of Oʻahu, Maui, and Hawaiʻi to explore how CWI (1) varies with different climate and vegetation characteristics, (2) affects plant water use and growth, and (3) contributes to water resources.
Results show that annual CWI varied from 158 to 910 mm, accounting for 3-34% of total water input at individual sites. This large variation was caused by differences in the quantity of cloud water, wind speed, and vegetation structure between sites. We developed a model to predict CWI using both climatic and forest canopy characteristics. On average, the model underestimated annual CWI by 18%, but reproduced the site differences relatively well. Plant water use decreased during periods of fog events mainly because of associated higher humidity. This new CWI model can be used to assess impacts of climate and land cover change on CWI and provide valuable information for resource management in Hawaiʻi, which was not previously possible.

At one field site, we explored the impacts of fog water on hydrological and ecological processes. Fog effects on native plant growth were indirect, primarily buffering effects of solar radiation. Removal of grass allowed natural regeneration of seedlings but did not alter soil moisture values. A soil data-collection program was initiated to help evaluate the role CWI has in providing moisture for plants, reducing wildfire risk within the fog

zone, and contributing to groundwater recharge to aquifers that supply drinking water and groundwater discharge to streams.

iii. TECHNICAL SUMMARY:

The goals of this study were to develop a process-based cloud-water interception (CWI) model to simulate the spatial patterns of CWI over the Hawaiian Islands, and improve understanding of the hydrological and ecological effects of fog and CWI on transpiration, plant growth and seedling recruitment, soil moisture, and groundwater recharge. Our study was divided into 3 parts summarized below:

1) CWI measurement and model- To develop a CWI model, we collected data at five sites that have different climate and different types of native Hawaiian tropical montane cloud forest (TMCF) ecosystems on three major islands in the Hawaiian archipelago. An empirical model relating CWI to cloud liquid water content (LWC), wind speed, canopy height and leaf area index (LAI) was formulated based on Katata et al. (2011) and tested against field observations. The Single Layer Wet Canopy Water Balance model (Takahashi et al. 2011) was used to calculate CWI from measured rainfall, throughfall, stemflow, and potential evaporation estimated by the Penman-Monteith equation (Monteith 1965). Because commercial LWC sensors are expensive and not suitable for use at remote field sites, we selected the Juvik-type fog gauge as a low-cost alternative to measure LWC. We conducted experiments to develop a method to remove errors due to wind-driven rain and to determine the gauge collection efficiency. LWC and the horizontal cloud water flux (CWF, linearly proportional to LWC times horizontal wind speed) were then calculated by analyzing collocated fog gauge, rain gauge, and wind sensor observations. We fitted the CWI model coefficients using observations of CWI and CWF at each field site and canopy structural variables obtained from field surveys and published data.

Our findings confirmed the high variability in both CWI and CWF over space and time. We found that about half of the variation in CWI could be explained by changes in CWF, and that the interception rate of cloud droplets by vegetation strongly depended on the canopy structure. When trying to predict CWI based on the observed CWF, the empirical CWI model underestimated the annual amounts by an average of 18% across sites. The model performed much better at some sites than others. The largest error (65%) occurred at a site with highly fragmented forest that largely enhanced the exposure of the canopy to wind-driven fog and rain. The enhanced fog capture in patchy vegetation was not well represented by the model. On the other hand, wind driven rain may have caused an overestimation of field-observed CWI, suggesting future research is needed to address the effects of forest patchiness to improve prediction accuracy.

The CWI model can provide valuable information about fog water input for purposes including studies about TMCF ecology and hydrology, water budget modeling, restoration, and water resource management. Passive fog gauges proved to be useful for low-cost LWC monitoring. The fog gauge calibration methods established in this study demonstrate how measurements from the widely-used Juvik-type fog gauges can be converted into LWC, which will greatly improve the comparability of TMCF studies across the world.

2) Ecological responses to fog immersion and CWI- Investigations on plant responses to fog immersion and CWI were conducted at the Nakula field site, a pasture to forest restoration site with remnant native trees on leeward Haleakalā. Sapflux measurements in native *Acacia koa* (koa) trees showed a strong relationship between tree transpiration and atmospheric dryness (vapor pressure deficit; VPD). We found that conditions at the leaf surface were highly coupled to the atmosphere, as fog decreased both atmospheric VPD measured at a climate station, and VPD at the leaf surface, contributing to decreased transpiration. Fog, which occurs mainly during the day at the Nakula site, also reduced solar radiation. Without fog, transpiration would be higher due to the effects of both higher VPD and higher stomatal conductance resulting from higher light levels. Trees at the Nakula site exhibited relatively high rates of nighttime sapflux, accounting for more than 35% of total daily transpiration. Because fog does not frequently appear at night, fog effects on nighttime transpiration were modest.

Another objective of this study was to identify the influence of fog immersion and CWI on the growth of saplings and trees at the Nakula forest restoration site and assess the recruitment of native seedlings under restoration activities. While fog supports plant survival and growth ecosystems elsewhere from the deserts of Namibia to coastal California redwood forests, its importance to the health of cloud-affected forests of the Hawaiian Islands remains unclear despite efforts to restore these ecosystems. Three years of continuous stem diameter monitoring (March 2016 - March 2019) of ʻaʻaliʻi (*Dodonaea viscosa, n=9*) saplings revealed nearly continuous growth (10 mm/year), with diameter increasing with higher rainfall and leaf wetness frequency, and decreasing in response to periods of higher VPD and net radiation although cloud water flux appeared to ameliorate this. Controls on growth of the much larger ʻōhiʻa (*Metrosideros polymorpha*) and koa trees were difficult to detect due to stronger diurnal and multi-day stem diameter variations. Despite this, periods of growth for the mature trees were positively associated with rainfall and cloud water flux and negatively associated with high VPD. Considered together, the results imply that additional moisture from rainfall and cloud water improved ʻaʻaliʻi sapling growth, while stem shrinkage of the larger, mature trees indicates that strong water deficit negatively affected tree water status and growth. Thus, potential decreases in cloud immersion and rainfall at this site are likely to have a negative effect on the growth of all the species considered.

We also monitored soil moisture (5 cm and 20 cm depth) and ʻaʻaliʻi germination and survival in plots where grass was removed and in paired control plots. In these experimental plots, which were in open areas (no trees), soil moisture was strongly influenced by periods of rainfall and mixed rain/fog events, but not fog-only events. Grass removal did not affect soil moisture at 20 cm, and effects at 5cm depth were inconclusive. The absence of larger trees above these plots meant that fog-associated

CWI inputs were minimal. In this open setting, fog served less as a precipitation input than a suppressant of evapotranspiration losses (by increasing air humidity and reducing solar radiation). The presence of grass appeared to contribute to a more rapid depletion of soil moisture; CWI on and through grass leaf blades likely did not exceed wet-canopy evaporation. Nevertheless, ʻaʻaliʻi seedling recruitment and survival was most strongly linked to grass presence/absence at time of germination, and not correlated with soil moisture. Although longer drying periods aligned with some mortality events, we did not have enough replication to evaluate the statistical significance of these events. Removal of grass likely reduced potential competition, allowing for ʻaʻaliʻi seedlings to germinate, and once established they can survive despite invasive grass regrowth. Findings also suggest that CWI and fog immersion may help seedlings survive long rainless periods by reducing evaporative demand and plant desiccation.

3) Soil moisture monitoring to link CWI with drought- A field data-collection program was initiated by the U.S. Geological Survey Pacific Islands Water Science Center (USGS-PIWSC) as part of a study to quantify the impacts of drought on water resources and the importance of CWI in mitigating the effects of drought. The overall objective of the USGS-PIWSC study was to provide information to (1) estimate changes in soil moisture, evapotranspiration, and groundwater recharge during periods of drought for current and projected climate conditions, and (2) estimate the combined effect of drought and reduced CWI on soil moisture, evapotranspiration, and groundwater recharge. To support the study objectives of the data-collection program, sensors for monitoring continuous soil water content and soil water potential were deployed at three CWI study sites: Nakula on the Island of Maui, and Laupāhoehoe and Nāhuku on the Island of Hawaiʻi, in collaboration with researchers from the University of Hawaiʻi at Mānoa Department of Geography (UHM). Soil samples were also collected from each of the sites during sensor installations and submitted for laboratory testing of soil physical properties. Additional data were collected to measure infiltration rates and soil physical properties at the Nakula study site. The measurements collected during the data-collection program are summarized in a USGS data release by Kennedy et al. (2019).

iv. PURPOSE AND OBJECTIVES:

Background - hydrological & ecological significance of CWI and fog

Persistent orographic lifting produces frequent fog on high tropical mountains, and forms hydrologically, biogeochemically, and ecologically important zones called Tropical Montane Cloud Forests (TMCF). Large amounts of water through the direct interception of liquid cloud droplets by vegetation canopies (cloud water interception, CWI) may be added to the TMCF system. Previous observations of CWI at four sites in Hawaiʻi indicated that CWI has great hydrological and perhaps ecological significance in Hawaiʻi. Cloud water (fog) as a moisture source in Hawaiʻi has been the subject of numerous studies since the mid-20th century (DeLay and Giambelluca 2011).

However, despite the long history of fog and CWI research, we still lack an understanding of fog and CWI patterns, and their variability over larger scales, that can be used to answer important hydrological and ecological questions, such as how CWI over the landscape contributes to water resources. This is both because direct measurement of CWI is difficult, and because the natural variability in CWI makes it challenging to scale up from a small number of observations (Giambelluca and Gerold, 2011). CWI is highly heterogeneous over space and time because of the variability in two major controls of the CWI process, namely the amount of cloud water that passes over the TMCF vegetation and the ability of the forest canopy to "capture" cloud droplets and transform it to an input to the water budget of the ecosystem. The atmospheric factors that determine the amount of cloud water that passes through a unit vertical area, called cloud water flux (CWF), are the liquid water content of the cloud and the wind speed that moves the cloud droplets. Vegetation characteristics such as height, density, and canopy architecture can influence cloud water interception and subsequent pathways such as interception loss (wet canopy evaporation), throughfall, or stemflow. In order to establish a large-scale understanding of the CWI patterns and make predictions for times and locations lacking direct observation, a model must be developed based on the knowledge of how different atmospheric and plant factors influence the CWI process.

Fog can play a large role in the water budget in Hawaiʻi (Scholl et al. 2007, Giambelluca et al. 2011), yet it is less clear how important fog water inputs are for native plant communities. Long-established work on coastal redwoods suggest that fog can affect plant growth (Dawson 1998) with implications for community assembly (Corbin et al. 2005, Fischer et al. 2009, Stanton et al. 2014). More recent research on TMCF species has established the importance of fog for supporting plant survival and growth through foliar water uptake (Eller et al. 2013) and other mechanisms including increasing moisture and altering light regimes (Bittencourt et al. 2019). For example, fog on the California Channel Islands provides soil water via fog drip that can be directly taken up by endemic pines, and also provides shade that ameliorates sunny drought conditions thereby lowering water loss from evapotranspiration (Fisher 2009). What is less well understood is how fog inputs can affect restoration efforts, although we note that managers have taken advantage of fog with collection structures to improve restoration success (Estrela et al. 2009). One study site on the Iberian Peninsula used such collection structures in combination with irrigation to increase pine and oak seedling survival. Nonetheless, the degree to which fog in such sites affects tree growth or seedling survival remains largely undocumented.

Rainfall is known to drive the recruitment of native species in arid environments and can thus have large effects on restoration success (Vieira and Scariot 2006, Yelenik and Levine 2010, Wainwright et al. 2012). This is particularly true in sites where managers use active seeding techniques or other treatments such as invasive removal to try and facilitate natural recruitment (Copeland et al. 2019). Variation in rainfall, then, can make or break project success, making high-cost restoration treatments risky if rainfall predictability is difficult. In fog-affected regions, it is possible that cloud water interception can increase soil moisture in ways that buffer periods of low rainfall. In addition, fog immersion can reduce evapotranspiration and water loss. This is not often quantified however, and the degree to which it can offset dry periods is largely unknown. In addition, competition from invasive species can interact with rainfall to alter restoration outcomes in unpredictable ways (Levine et al. 2008, Wainwright et al. 2012). This is at least in part due to invasive species often being water limited in dry ecosystems, yet better able to quickly take up resources, making outcomes in high precipitation years unpredictable.

Goals of the study

The goals of this study were to develop capability to characterize CWI for a range of vegetation types and climatic conditions and improve understanding of the hydrological and ecological effects of CWI in Hawaiʻi. As part of a larger effort, this study is intended to lead to the development of CWI maps, estimates of CWI-derived groundwater recharge, and maps of the regional soil moisture distributions for different climate and vegetation conditions, which can provide useful information for water resource management and ecological restoration.

Objectives

Objectives of this research included: (1) determine, from field measurements, cloud liquid water content (LWC) and wind speed (WS) at TMCF sites across Hawaiʻi; (2) test regional model simulations of horizontal flux of cloud liquid water (CWF, derived from LWC × WS); (3) test low-cost alternatives for measuring LWC; (4) determine, from field measurements, cloud water interception; (5) develop and test an empirical model relating CWF and vegetation characteristics to CWI; (6) estimate the effect of fog on transpiration via leaf wetting; (7) relate temporal variability of CWI and broader environmental conditions to seedling recruitment and survivorship; (8) conduct measurements of plant growth to determine the overall effects of fog on ecosystem health; and (9) collect field measurements of soil water content and soil water potential for a related study that will (i) develop regional estimates of soil moisture using a water budget model, (ii) contrast soil moisture from areas with and without CWI to evaluate the importance of CWI during periods of drought, and (iii) estimate plot-scale groundwater recharge rates.

Changes made and reasons

1) CWI measurement and model (objectives 2 and 3)

The original objective of testing several low-cost alternatives for measuring LWC was narrowed down to calibrating the Juvik fog gauge to measure LWC. This is because installing a LWC sensor at one of the field sites was found to be impractical and the fog gauge had to be calibrated separately. As a result, two additional experiments were added to collect calibration data for the Juvik gauge; other alternative methods of fog monitoring were not extensively examined. The planned testing of regional climate model simulation of CWF has not yet been completed because of the unavailability of climate model output data. We will continue to pursue this objective.

2) Ecological responses to fog immersion and CWI (objective 8)

In a study that went beyond the original objectives stated in the proposal, we conducted measurements of plant growth to determine the overall effects of fog on ecosystem health. This was done to make use of recently tested automated dendrometer sensors and methods that allow for the measurement of real-time plant growth in relation to local environmental conditions. Continuous and non-invasive sensing of plant diameter growth at restoration sites can provide a metric of the effectiveness of various out-planting and restoration practices. The CWI study at the Nakula Natural Area Reserve on the island of Maui provided a valuable opportunity to investigate native plant performance and restoration effectiveness at a cloud-affected forest site. Automated dendrometers stand to offer powerful tools for asking questions that relate to plant physiology, ecology and ecohydrology in remote habitats. We asked the following questions focused on understanding the growth of native shrub and tree species at this pasture-grass dominated site:

1. Which climatic factors influence growth of juvenile ʻaʻaliʻi (*Dodonaea viscosa*) during the study period? Specifically, to what extent are cloud water inputs associated with growth?
2. Which climatic factors influence growth of mature koa (*Acacia koa*) and ʻōhiʻa (*Metrosideros polymorpha*)?
3. How does the removal of dense, non-native grass affect cloud water effects on soil moisture and ʻaʻaliʻi (*Dodonaea viscosa*) seedling natural recruitment, growth, and survival?

We installed automated dendrometers to continuously monitor plant growth as stem diameter in a field study focusing on forest cloud water inputs to address questions 1 and 2 above. We also installed shallow and deeper soil moisture and microclimate sensors across an array of grass removal (treatment) and control plots at the same field site (question 3). Finally, we monitored natural ʻaʻaliʻi recruitment in grass removal and control plots (question 3).

To-date, few automated dendrometers have been deployed in the Hawaiian Islands. The stem radial variation as recorded by these sensors captures both diameter growth and variations in tree water status. Untangling these different signals has been the basis of numerous dendrometer-based studies since the relative strength of the cambial growth signal vs. water status signal varies across environments, seasons, species, sensor types and installation details (whether bark was removed, etc.). Except for the seasonally dry tropics (Spannl et al. 2016), the absence of a distinct growth-limiting cold season in tropical environments can complicate interpretation of automated dendrometer time series data. Trees in tropical humid or otherwise less seasonal environments tend to show more continuous growth associated with multiple climatic or environmental factors (Bräuning et al. 2009). Furthermore, growth patterns are species-specific and can operate on different scales of time (Köcher et al. 2012). Untangling controls on tree diameter growth and organism-scale productivity in these contexts remains an important challenge to understanding the future of cloud forest species and community dynamics in the face of climate change.

3) Soil moisture monitoring to link CWI with drought (objective 9)

A field data-collection program was conducted as part of a study to quantify the impacts of drought on water resources and the importance of cloud-water interception (CWI) in mitigating the effects of drought (see https://cascprojects.org/#/project/4f8c650ae4b0546c0c397b48/580f8424e4b0f497e795ffe1 for study goals and objectives).

To support the objectives of the data-collection program, a set of sensors for monitoring continuous soil water content and soil water potential were deployed at three of the CWI field study sites: Nakula, Laupāhoehoe, and Nāhuku. A set of soil samples was also collected from each of the study sites during the sensor installations and submitted for laboratory testing of soil physical properties. Additional data collection to measure infiltration rates and soil physical properties was conducted at the Nakula study site.

v. ORGANIZATION AND APPROACH:

1) CWI measurement and model

To develop a process-based CWI model, we first measured and compared CWI at sites spanning numerous climate conditions and TMCF ecosystem types across the Hawaiian Islands. The relationship between CWI and the selected meteorological and canopy structure variables, namely LWC, wind speed, canopy height, and leaf area index, was used to model CWI based on a previous study by Katata et al. (2011). We tested this CWI model by comparing the model to the CWI field observations and adjusted the model parameters to fit the characteristics of the vegetation in Hawaiian ecosystems.

Field sites

We made field observations of CWI and related variables at five sites on three different islands of Hawaii. Since four of the five field sites had existing climate stations, we only required a new climate station at Nakula (Figure 1, Table 1). The climate station at each site measured a wide range of variables including air temperature and relative humidity, wind speed, rainfall, 4-component net radiation (incoming and outgoing solar and longwave radiation), soil heat flux, and soil moisture. For this study, we upgraded all climate stations to include a Juvik-type passive fog gauge, two trough-type throughfall gauges, a variable number of stemflow gauges (one each at Nakula, Laupāhoehoe, and Nahuku; three at Kaʻala and ParkHQ), three leaf wetness sensors, and one digital trail camera. At Nahuku, Laupāhoehoe, and Nakula, we added soil moisture profile sensors

and tensiometers (which measure soil water status) placed under tree canopies at multiple depths. We also installed sap flow sensors at Nakula to measure transpiration of *Acacia koa* (koa) trees. Figure 2 shows the field site layout. The project study period occurred from July 2016 – December 2020.
All CWI-related abbreviations, acronyms, and symbols are defined in Appendix A.

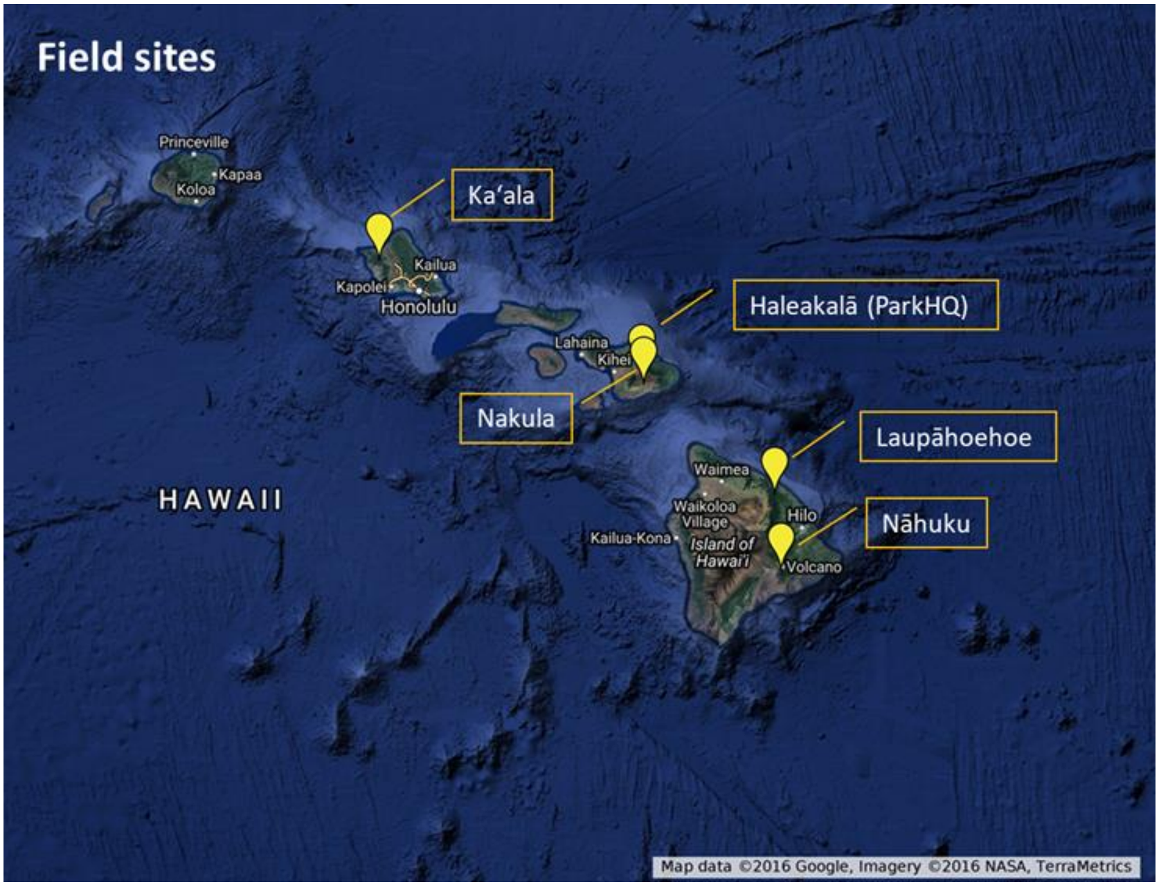

Figure 1. Field site locations.

Table 1. Field site characteristics. MAR = mean annual rainfall.

Station	Island	Elevation (m)	MAR (mm)	Vegetation type	Canopy height (m)	Species
Kaʻala	Oʻahu	1208	1937	Montane cloud forest	3	ʻōhiʻa
Laupāhoehoe		1100	3375	Wet rainforest	27	ʻōhiʻa; koa
Nakula	Maui	1645	1805	Fragmented mesic forest	15	koa
ParkHQ	Maui	2114	1155	Sub-alpine shrub	2	pukiawe
Nāhuku		1201	2754	Wet montane forest	18	ʻōhiʻa; olapa

Liquid water content – passive fog gauge as the low-cost alternative

One of the major drivers of CWI is the horizontal flux of cloud water (CWF), which is directly related to the product of cloud liquid water content (LWC) and horizontal wind speed (Giambelluca et al. 2011a). Most LWC sensors are expensive and not suitable for long-term monitoring at remote field sites; therefore, a low-cost, simple-to-use alternative was needed to measure fog and LWC at multiple sites in TMCFs in Hawaiʻi. We used the louvered aluminum screen fog gauge with rain shield (hereafter, Juvik gauge) described in Hansen and Juvik (2010). The Juvik fog gauges were successfully used in earlier studies in Hawaiʻi to measure fog (Juvik and Nullet 1995). The rain shield prevents most vertical precipitation, and the cylindrical screen ensures that collection efficiency is not affected by varying wind direction. In order to use the Juvik gauge to measure LWC, we first calibrated the Juvik gauge for the errors associated with non-vertical wind-driven rain (WDR) and the gauge's efficiency in collecting cloud droplets.

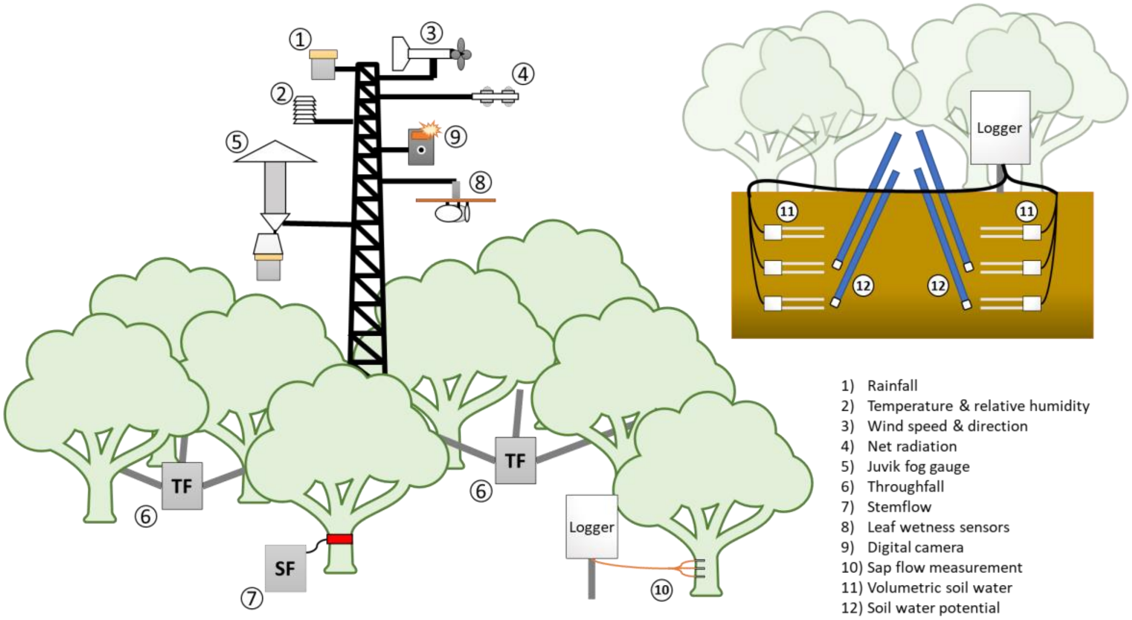

Figure 2. Field site instrumentation layout.

The raw fog gauge measurements, or the volume of water collection measured by the fog gauge, was first separated into the contribution of fog water catch and the WDR catch (Appendix B, equation 1). After removing WDR, the fog water catch was converted into CWF and LWC by adjusting for wind speed, collection area of the fog gauge, and the fog gauge efficiency (Appendix B, equations 2-3).

Two separate experiments were conducted to (1) establish a method to estimate WDR errors in the fog gauge data using rain intensity and wind speed data and (2) to determine the gauge-type-specific collection efficiency.

For the WDR error correction, we collected calibration data on the roof top of a building on the campus of University of Hawaiʻi at Mānoa during March – December 2020, and established a method to estimate WDR catch using WS and hourly rain rate based on widely used models of terminal velocity and raindrop size distribution (DSD). The terminal velocity equation (Atlas et al. 1973) and the raindrop size distribution function (Marshall and Palmer 1948) were validated with raindrop diameter and velocity data measured using a laser disdrometer (Nanko et al. 2006). The raindrop DSD, terminal velocity, and wind speed were used to calculate the fall angle of each raindrop size class. The theoretical WDR was calculated as the total volume of raindrops that would fall into the Juvik gauge collector. We then compared the calculated theoretical WDR to the actual WDR measured by a Juvik gauge under fog-free conditions to check and adjust the WDR error correction method.

To determine fog gauge collection efficiency, we compared the Juvik gauge measurements to a highly sophisticated cloud droplet sensor called Flight-Probe Dual-Range Phase Doppler Interferometer (PDI, Chuang et al. 2008). Because PDI was built for cloud physics studies on aircraft, we designed a mobile station to adapt the PDI instrument to collect accurate LWC measurements under field conditions at Mt. Kaʻala during April – July 2018 to serve as the reference value (Figure 3, Appendix C). The Juvik gauge data was converted to LWC using the wind speed and rain gauge data from the mobile station. We estimated the fog gauge efficiency by comparing the fog gauge-derived LWC to the reference LWC using linear regression.

Figure 3. Instrumentation: (1) Phase Doppler Interferometer (Artium Technologies, Inc.), (2) Cloud Droplet Probe (Droplet Measurement Technologies, Inc.), (3) Juvik fog gauge, (4) visibility sensor, (5) rain gauge, (6) wind speed and direction monitor, (7) digital camera, (8) water isotope sampler, (9) aerosol spectrometer, (10) UAV sensor.

Fog occurrence, CWF, and LWC at the five field sites were monitored by the Juvik fog gauge installed near the climate station at each site. The gauge efficiency and WDR error correction method were used to calibrate the fog gauge measurements with data from the collocated rain gauge and wind speed sensors. Extreme values in CWF were removed when the rain rate exceeded 10 mm/hr, or wind speed (at fog gauge height) exceeded 5 m/s, values which caused large errors in WDR estimation. The data were aggregated to produce hourly time series datasets for each site, and erroneous values and outliers were removed by filtering out environmental conditions of wind speed and rain which tend to cause large errors. Annualized values were calculated from the average of the study period, and LWC was averaged both over the entire study period and only during the hours of fog events when CWF > 0.01 mm.

Cloud water interception - estimated by canopy water balance

We used the Single-Layer Wet Canopy Water Balance model (SLWCWB, Takahashi et al. 2011) to estimate CWI. The canopy water balance can be described according to:

$$RF + CWI = TF + SF + E_i + \Delta S$$

where *RF* is rainfall, *CWI* is cloud water interception, *TF* is throughfall, *SF* is stemflow, *Ei* is evaporation from the wet canopy, and *ΔS* is the change in the canopy water storage.

All terms were in units of mm. The SLWCWB model uses data of RF, TF, SF, potential evaporation (PE), and two canopy parameters, canopy water storage capacity and free throughfall ratio, to calculate canopy water balance and tracks the canopy water storage at each time step to estimate CWI and Ei. We measured RF, TF, and SF directly at each site using automated recording gauges. PE was estimated using the meteorological data measured at the climate station based on the Penman-Monteith equation (Monteith 1965).

The canopy parameters were estimated by analyzing cumulative RF, TF, and SF of selected events using a method similar to Takahashi et al. (2011) (see Appendix D for methods). Events were identified as periods separated by more than 3 hours of no RF, TF, or SF.

In a preliminary study, we compared several versions of the SLWCWB model, using field data from Nakula, to test the effects of modifications in the model configuration. We selected two versions (named SL3 and SL4) which differ from the original model in the treatment of negative values of potential evaporation and the order of calculating evaporation versus drainage from the canopy storage. We report the average values from both model versions.

The SLWCWB model was run independently for each site. For those sites having different recording frequency for some variables, the time series data were aggregated to the interval of the smallest common multiple at that site. Finally, the model output of CWI, E_i, and related variables were aggregated to produce an hourly data set for each site.

Cloud water interception empirical model

Two main factors affecting CWI were the amount of cloud water, measured by CWF, and the ability of the vegetation canopy to intercept cloud droplets. We followed Katata et al. (2008 and 2011), where CWI can be predicted as the product of CWF and the interception rate of the vegetation (A), where A is dependent on the ratio of canopy height (h) to the total leaf area per ground area (leaf area index, LAI). Additionally, we inferred that the interception rate increased nonlinearly with taller vegetation and relatively loosely distributed leaves vertically throughout the canopy because of a higher chance for wind carrying cloud droplets to penetrate into the canopy (Katata et al. 2011). However, this relationship also depends on other factors such as vegetation type and plant species.

We used data from major Hawaiian ecosystems in the cloud zone to estimate the values of CWI model coefficients. LAI data were obtained from the Evapotranspiration of Hawaiʻi website (Giambelluca et al. 2014). Canopy height, or the average height of the taller trees for the Nakula and ParkHQ sites, was obtained from field survey and published data (Ostertag et al. 2014). The values of the interception rate of vegetation (A) at each site were estimated by comparing observations of CWI to CWF using linear regressions. For Nakula and ParkHQ where forest canopies were not uniform, CWI calculated by the SLWCWB was only valid for the areas under the patches of tall vegetation where TF and SF were measured, and was scaled by percent canopy cover to a per ground area basis. Canopy cover at Nāhuku, Laupāhoehoe and Kaʻala was assumed to be 100%, and estimated for the Nakula and ParkHQ sites. We surveyed the vegetation at ParkHQ in two 10 m x 10 m plots to estimate the percentage of land covered by plants versus bare ground. Each plot was divided into a 10 x 10 grid (grid size 1 m^2), and the grids that had living plants located at the center were counted for each plot. Then, the canopy cover was estimated by dividing the number of grids with live plants by the total number of grids. For Nakula, canopy cover was estimated by visually inspecting images from Google Earth. A sample area of 1 km × 1 km was divided into four 500 m x 500 m plots, and each plot was further divided into a 10 × 10 grid (grid size 50 m × 50 m). The number of grids with more than 50% tree cover was counted and divided by the total grid number to estimate the canopy cover in each plot, and the canopy cover over the sample area was calculated as the average across the four plots.

We fitted the CWI model by comparing the interception rate estimated from the observed relationships between CWI and CWF to that predicted by canopy height and LAI based on the model by Katata et al. (2011). We then evaluated the model fit and performance using root-mean-square error, and compared CWI predictions to the measured CWI values.

Leaf wetness sensor data

We installed three leaf wetness sensors (PHYTOS31, METER Group, Inc.) next to the Juvik fog gauge at each site. Sensors were secured under a rain shield to exclude effects of rain, and oriented to detect cloud water flux coming from different directions. The original leaf wetness sensor output gives the number of minutes during which the sensor was at one of three wetness levels (i.e., wet, dry, in-between) as three separate variables. We condensed the sensor output into a proportion time wet (LWS_{ptw}) metric which is a weighted average of the three wetness levels, with values ranging from 0 to 1, with 0 meaning the sensor was dry throughout the period and 1 meaning the sensor was wet throughout the period. We calculated LWS_{ptw} for each leaf wetness sensor and then calculated the average of three sensors to represent the site condition. The average LWS_{ptw} was used (1) in the preliminary tests of canopy water balance models to compare with model predictions of canopy water storage due only to CWI, and (2) the identification and categorizing of precipitation event types, which was used in the analyses of plant responses to fog.

Precipitation event type identification

For the analyses of sapflux measurements (used to estimate tree-level transpiration), dendrometer data, and grass removal effects on soil moisture, we divided data periods into events of different precipitation types, post-event periods, and non-event periods. We interpolated event data to align with the time-series of sapflux measurements. We identified precipitation events based on data from rain gauge, Juvik fog gauge, and leaf wetness sensors. Precipitation events were defined as periods separated by more than three hours of: rainfall = 0, fog water catch = 0, and $LWS_{ptw} < 0.5$. Note that this is different from event identification for canopy parameters analyses described earlier. We then identified a three-hour window following each event (post-event) when the canopy was assumed to remain at least partially wet. All remaining time steps were considered non-event periods. We further categorized events by precipitation types into rain-only, fog-only, and rain+fog. Fog presence was determined by fog gauge, the leaf wetness sensors, or both.

2) Ecological responses to fog immersion at Nakula

Site context and microclimate

The Nakula NAR was previously grazed, but following ungulate eradication in 2013, has been the site of large-scale outplanting by the DLNR Division of Forest and Wildlife Native Ecosystem Protection and Management program and the Maui Forest Bird Recovery Project (MFBRP; Warren 2019). We chose this site because, given its lower annual precipitation than other sites, plants were more likely to be water limited, and thus show responses to CWI. The study site was dominated by introduced pasture grasses, patches of remnant native canopy species koa (*Acacia koa*) and ʻōhiʻa (*Metrosideros polymorpha*) and naturally regenerating ʻaʻaliʻi (*Dodonaea viscosa*) which are increasing in abundance due to restoration activities such as fencing, ungulate removal, and herbicide/weed whacking treatments. Figure 4 shows the koa stand where the soil moisture and soil water potential sensors were installed, the Juvik fog gauge, and the rain gauge at the climate station. Details of these measurements are described in the earlier sections. Relative humidity and air temperature values, collected at each climate station, were used to calculate vapor pressure deficit (VPD).


Figure 4. Image of koa-dominated patch and grass-dominated understory.

Fog effects on transpiration

We used sapflux density measurements to estimate transpiration rates for 12 koa trees at the Nakula site. We installed heat ratio method sap flux sensors (Burgess et al. 2001) at breast height (1.3m) to measure transpiration. Each sensor consisted of a central heater probe, and two temperature sensor probes installed horizontally into the stem above and below the central heater probe to measure xylem temperature. The distance between the heater probe and each temperature-sensor probe was 6 mm. Each probe was made of a stainless tube (1.2 mm in outer diameter), with coiled Ni-Cr wire (20 ohm) inside the heater probe. Each temperature-sensor probe contained two thermocouples, one installed at 1 cm and another at 2 cm from the surface of the xylem. Heater probes were connected to a power board, and emitted a heat pulse at 10-min intervals. Temperature-sensor probes were connected to a multiplexer (AM16/32, Campbell Sci., Logan UT, USA), which was connected to a data logger (CR1000, Campbell Sci.). Xylem temperature was measured before heat pulse and 60-100 s after the heat pulse.

Means of xylem temperature before and after heat pulse were calculated to determine heat pulse velocity (HPV, a measure of transpiration rates) (Burgess et al. 2001). We used net radiation values from climate stations to evaluate HPV measurements across different categories of net solar radiation.

Dendrometer measurements

We examined the fluctuation of stem size using digital tree dendrometers which allowed us to link individual-level high temporal resolution growth responses of trees to environmental conditions monitored at each site’s climate base station. We monitored growth of ‘a‘ali‘i (*Dodonaea viscosa*) shrubs (n=9) between 1 and 5 cm basal diameter using small diameter dendrometers (DD-S model, Ecomatik, Germany). We specifically targeted ‘a‘ali‘i that recruited as a part of an earlier restoration study. We selected three individuals in each of three different 5 m × 5 m restoration plots where grass was killed with herbicide, and then three months later the dead grass biomass was removed to expose soil (Warren et al 2019). Shrubs were approximately three years old at the start of the study. Within each plot, we chose ‘a‘ali‘i individuals that were average to above average in size (based on observation) and were not directly next to each other. We placed the dendrometer on the main stem about 30 cm from the soil surface and cleared away grass from the immediate area so it would not interfere with the device (Figure 5).

Figure 5. Close up of the small-sized dendrometer on ‘a‘ali‘i stem and side view of plot showing multiple ‘a‘ali‘i approximately 2 m tall, with exotic grass understory and the data logger. Note fog in the background.

We also banded mature ‘ōhi‘a trees (n=5) and koa trees (n=4) varying in size from 40 to 80 cm DBH using circumference dendrometers (DC3 model, Munich, Germany). We removed loose bark before attaching dendrometers so that it would not interfere with measurements as it shifted or fell off (Figure 6). The monitored individuals were located across three sites at the Nakula NAR that were separated from each other by natural terrain such as gulches (Appendix F). Measurements spanned the period from March 2016 to March 2019 and were logged at 15-minute intervals. While sensors had some gaps in operation, most data were relatively continuous, and we did not attempt to gap fill.

Figure 6. Dendrometer installation on a large koa individual (Photo by Stephanie Yelenik).

Dendrometer data analysis

We used the growth line approach to summarize data for analyses (Zweifel et al. 2005, Ehrenberger et al. 2012, Oberhuber et al. 2015). This method characterizes diameter growth as a one-way process, modeling the running maximum diameter as a step function (the “growth line”). We focused analyses on progressive increases in cumulative maximum diameter, which we assumed represented real growth (RG). We also calculated stem radius variation, a measure of plant water deficit (WD) as the difference between this growth line and hourly median diameter data. This metric provided a means to assess multi-day shrinkage events. We focused on ‘a‘ali‘i RG because it had a minimal bark swelling effect, but we looked at WD to better understand the diameter fluctuations of the larger ‘ōhi‘a and koa trees. Additional methods regarding data preparation can be found in Appendix G.

To assess species responses to climate, we created a binomial daily RG series dataset (‘a‘ali‘i only) by classifying each individual as exhibiting either diameter increase (1) or no change (0) over the 24-hour period of a given day. We also created weekly metrics of RG and WD for all species. We rescaled our daily RG series by dividing each individual by their respective initial stem diameters, then pooled individuals to calculate a species mean and standard deviation for RG and WD. We used the WD standard deviation data to identify and remove individual outliers. Weekly species RG and WD were calculated by summing the rescaled species mean daily observations over weekly intervals.

We used multiple logistic regression to understand how environmental conditions influenced daily ‘a‘ali‘i RG, following methods outlined in Ziaco and Biondi (2018). We also created a contingency table comparing binomial daily ‘a‘ali‘i RG to days classified by precipitation type (clear, fog only, rain only, and fog + rain). We used multiple linear regression to examine weekly RG of each species, and weekly WD for ʻōhiʻa and koa, as a function of continuous environmental covariates.

We used environmental measurements from the climate and soil moisture monitoring stations as covariates. We assessed correlation among variables and removed redundant predictors. When necessary, we transformed predictor variables to ensure normality/homoscedasticity, using the bestNormalize R package (Peterson 2019). We explored a subset of predictor variables to identify those with particularly strong influence on the binomial RG response using the hierarchical partitioning package hier.part (MacNally and Walsh, 2004). We used the MuMIn R package (Barton 2020) for all regression analyses, and conducted model selection using methods by Burnham and Anderson (2002). We identified and disregarded models suffering from term collinearity by assessing variance inflation factors calculated using the car package (Fox and Weisberg 2019). Analyses were conducted in an R environment (R Core Team 2020).

Seedling recruitment and survival

We monitored the seedling dynamics of the native shrub ʻaʻaliʻi with the intention of relating seedling emergence and survival of this species to cloud water input, rainfall, and soil moisture. Previous research by MFBRP showed that using herbicide on slopes that are dominated by exotic pasture grasses and following that treatment with grass biomass removal leads to natural recruitment of ʻaʻaliʻi. We monitored seedling emergence, survival, and growth in three treeless sites that were treated with herbicide and cleared of grass biomass in April 2016 (“Spray 6”), July 2016 (“Spray 4”), and August 2016 (“Spray 2”), as well as in adjacent, untreated sites still dominated by exotic grasses. Treatment areas were approximately 30 m × 30 m in size, and plots were dispersed regularly through the area. We created five 1 m × 1 m plots in both grass removed and grass intact treatments at Spray sites 2, 4 and 6 for a total of 30 plots. In each plot, we counted ʻaʻali’i seedlings in five separate size classes (0 – 5 cm, 5 – 10 cm, 10 – 30 cm, 30 – 100 cm, and over 100 cm). Because we did not track each seedling individually, counts represent the net effect of recruitment and mortality at any given time point. Plots were censused eight times over 2.5 years (April, July, September, and December 2016, May and August 2017, January and September 2018). To target survivorship and growth rates more precisely, we also marked 30 ʻaʻaliʻi seedlings per site in the grass removal treatment. These were regularly dispersed within the cleared area. We did not include seedlings from the control/grass intact treatment because we did not find any during site visits. At the same census dates noted above, we monitored seedlings for survival, height to the apical meristem, and measured width at the widest point of the individual. We also noted if grass had regrown around the individual as a binomial presence/absence variable. We used logistic regression to investigate whether individual survivorship is affected by grass presence/absence. Finally, at each site, we installed one soil moisture sensor at each of two depths (5 and 20 cm) in both treatments (with grass, and grass removed) to track soil moisture over time.

3) Soil moisture monitoring to link CWI with drought

Soil-moisture sensor installations and soil-core sampling at Nakula, Nāhuku, and Laupāhoehoe

Soil-moisture sensors were installed at three sites including Nakula on the island of Maui, and Nāhuku and Laupāhoehoe on the island of Hawaiʻi between July 2016 and July 2017, for measuring soil volumetric water content and soil water potential (Figure 8). See Appendix H for installation details. In January and February 2018, reflective insulation was used to cover the exposed parts of the refill lines of the soil water potential sensors at each site to minimize the effects of daytime heating on soil water potential measurements. Soil-moisture sensor data collection, storage, and management was led by UHM.

A set of soil-core samples was collected during the installation of the soil volumetric water content monitoring sensors at each study site. A description of the soil-core sampling procedure is presented in a USGS data release by Kennedy et al. (2019) (see processing step 1 in metadata https://doi.org/10.5066/P9J5SESD). All samples were tested for physical properties including dry bulk density, porosity, volumetric water content, gravimetric water content, and particle-size distribution at a USGS laboratory in Menlo Park, California, and described in Kennedy et al. (2019).

Figure 8. Soil-moisture measurement locations at (a) Nāhuku, Hawai‘i (photo from Joseph Kennedy), (b) Laupāhoehoe, Hawai‘i (photo from Han Tseng), (c) Nakula, Maui (photo from Alan Mair). S-1 and S-2 indicate soil moisture sensor locations.

Soil infiltration-rate, hydrophobicity, and preferential-flow measurements and surface soil sampling at Nakula

Additional data collection was conducted at the Nakula site in January 2018 to assess soil infiltration rates, hydrophobicity, and preferential flow (Appendix I). The Nakula site had two plots, each of which contained 15 or 17 individual measurement locations. A central measurement location was installed, with additional locations installed in a concentric arrangement. These procedures are further described in Kennedy et al. (2019) (see the summary file of tables and maps, and processing steps 3 to 7 in metadata https://doi.org/10.5066/P9J5SESD). Soil samples were processed for particle-size distribution at a USGS laboratory in Menlo Park, California.

vi. PROJECT RESULTS:

1) CWI measurement and model

Raindrop characteristics

The raindrop size distribution function, hereafter MP model, (Marshall and Palmer 1948) described the raindrop drop size distribution well under moderate intensity rain (see

Appendix K, Figure 1). The MP model underestimated raindrop count during heavy rainfall; however, this may be the result of disdrometer measurement error. The disdrometer can underestimate drop counts if multiple raindrops overlap when passing the laser sensors, which is more likely to happen during heavy rainfall due to the large drop size. The MP model also appeared to underestimate the raindrop count of light rain (RI = 1 mm/hour), and bias toward larger drop sizes. This higher concentration of small raindrops may be a characteristic of the Hawaiian orographic precipitation (Blanchard 1953). Closer examination was impossible with the existing data because raindrops smaller than 0.75 mm were not measured due to the limitation of the disdrometer, and future research is needed.

The relationship between raindrop diameter and velocity measured by the disdrometer was matched reasonably well by the model (Figure 9).

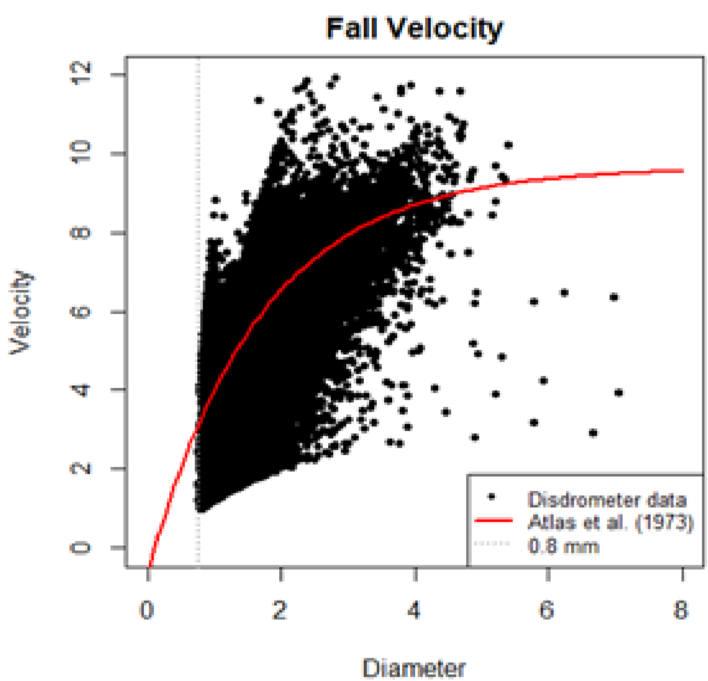

Figure 9. The relationship between raindrop diameter and fall velocity measured by the disdrometer and predicted by different terminal velocity function (Atlas et al. 1973).

Wind-driven rain correction method

We developed a method to estimate wind-driven rain (WDR) errors by first calculating the theoretical WDR errors, or amount of WDR that would enter the fog gauge, and then adjusting the timing and values for biases.

The comparison of the theoretical WDR errors calculated based on modeled terminal velocity and raindrop size distribution models to the observed WDR errors measured by the Juvik gauge data revealed many instances of overcorrections in the dataset

(Appendix K, Figure 2). Most overcorrections were caused by 1) the lagged response of the fog gauge when compared to the rain gauge and 2) the tipping-bucket resolution of the fog gauge. Further details about WDR correction and Juvik gauge collection efficiency methods can be found in Appendix K. See Appendix L for the look-up table of Juvik gauge exposed area and raindrop trajectory angle.

Field observations: fog gauge-derived variables

Fog occurrence, LWC, and cloud water flux (CWF) at each field site was monitored by the Juvik fog gauge. The total water collection recorded by the Juvik gauge was analyzed with the collocated rain gauge and wind speed data to separate fog water catch and wind-driven rain catch, and CWF and LWC was then calculated from fog water catch values (Appendix B).

Fog frequency and fog gauge water collection

The annualized values of fog gauge-derived variables are summarized in Table 3. The frequency of fog occurrence, defined as the percentage of hours when CWF > 0.01 mm/hour, was highly variable across sites. The highest fog frequency was observed at Mt. Kaʻala where fog was observed close to 60% of the time, which was more than 3 times as high as rain. The lowest fog frequencies were observed at Nakula and ParkHQ. This can be explained by the location of these two sites: Nakula is situated on the leeward side of Haleakalā; and ParkHQ is at the elevation near the base of the trade wind inversion.

Total water collection by the Juvik gauge ranged from 10.5 L at Nakula to 520 L at Mt. Kaʻala annually. Approximately 70 – 90% of the water collected by the Juvik gauge was due to fog across all sites except for Laupāhoehoe, where fog contributed about 40% (Figure 10). This variation is partly due to the differences in wind speed at the fog gauge height because increased exposure to wind increases the water collection in general. For example, Nakula and ParkHQ had similar fog frequency and liquid water content, but fog water catch (FOG) was much lower at Nakula due to the low WS.

Cloud water flux and liquid water content

Large between-site variation was also found for CWF, which is closely related to fog water catch (FOG). Variation in the FOG-CWF relationship was due to WS differences between the height of the fog gauge and the canopy. The annualized CWF was higher than RF at all the sites except for Laupāhoehoe, and the highest CWF was found at Mt. Kaʻala and Nāhuku where the values were close to 32,000 mm and 15,000 mm per year, respectively. Annual CWF was disproportionate to annual RF, meaning a site with low RF does not necessarily have low CWF. It is worth noting that, although comparing CWF to RF to imply the significance of fog as a water source is a common practice, CWF is not equal to cloud water interception (CWI) when calculating a water budget. The difference between RF and CWF patterns showed that observations by traditional rain gauges alone do not accurately capture the moisture availability of TMCF sites in Hawaiʻi (Table 3).

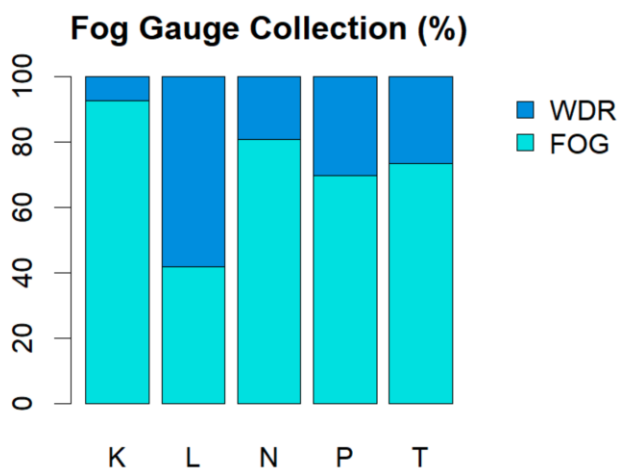

Figure 10. Percentage of fog water (FOG) versus wind-driven rainwater (WDR) collected by the Juvik gauge at each site, estimated using the WDR correction method, at each field site. K = Ka‘ala, L = Laupāhoehoe, N = Nakula, P = ParkHQ, T = Thurston (Nāhuku).

Table 3. Annualized amounts and ratios of selected variables.
FC = total water collection by fog gauge; TF = throughfall; SF = stemflow; RF+CWI = total precipitation; Ei = evaporation from wet canopy; PE = potential evaporation; Rnet = net radiation; Tair = air temperature; RH = relative humidity. CWI and Ei (evaporation from wet canopy) are shown as the average of model version SL3 and SL4. See text for the definition of RF, CWI, and fog frequency.

Variable	Unit	Kaʻala	Laupāhoehoe	Nakula	ParkHQ	Nāhuku
RF Frequency	%	16.2%	26.3%	9.3%	9.0%	25.3%
Fog Frequency	%	46.7%	24.0%	23.1%	14.2%	35.5%
CWI Frequency	%	60.2%	18.2%	6.7%	9.3%	30.8%
RF	mm	1806.0	5520.8	1805.3	1124.3	3020.1
FC	L	520.1	63.1	10.5	56.9	219.3
WDR Collection	L	39.5	36.8	2.0	17.3	42.8
Fog Water	L	483.2	26.3	8.5	39.6	117.9
CWF	mm	31669.3	3067.1	2057.0	5656.6	14801.2
CWF/RF	%	1753.6%	55.6%	113.9%	503.1%	490.1%
TF	mm	2184.4	4804.3	2121.3	527.7	2764.2
SF	mm	172.5	580.1	15.9	79.0	160.7
CWI	mm	910.7	157.8	604.6	565.5	859.6
RF+CWI	mm	2716.7	5678.6	2410.0	1689.8	3879.7
CWI/(RF+CWI)	%	33.5%	2.8%	25.1%	33.5%	22.2%
Ei	mm	313.8	437.2	246.7	236.3	359.3
PE	mm	955.0	1033.4	810.3	1150.7	1346.9
Rnet	W/m2	109.5	114.8	90.6	131.9	144.4
Tair	°C	14.9	16.3	14.4	12.5	15.5
RH	%	95.7%	86.7%	78.2%	65.4%	93.1%
LWC	g/m3	0.66	0.06	0.04	0.07	0.20
LWC (during fog)	g/m3	1.07	0.32	0.65	0.72	0.60
WS	m/s	2.42	2.46	0.99	2.30	4.35

The extremely high CWF at the Kaʻala site was surprising even though large fog water input was expected. Underestimated collection efficiency of the Juvik gauge may have introduced biases when converting FOG to CWF. The highly persistent fog at Kaʻala may also increase the gauge collection efficiency by reducing evaporation from the collector screen. The collector screen was found partially covered by a layer of lichen-like organism toward the end of the experiment. This may also have changed the collection efficiency although the direction of change is unknown and no clear effects could be detected from the data.

The mean LWC during fog events, averaged at 0.67 g/m^3, was relatively consistent across the sites while the mean LWC across all weather conditions during the study period varied by over an order of magnitude. The low LWC during fog found at Laupāhoehoe can be explained by its low elevation near the lower edge of the cloud zone where fog is less frequent.

Field observations: cloud water interception

The annualized values of CWI estimated by both versions of the SLWCWB are summarized in Table 3. The mean annual CWI ranged from 157 mm at Laupāhoehoe to 910 mm at Kaʻala. The ratio of CWI to total precipitation (RF + CWI) ranged from less than 3% at Laupāhoehoe to over 33% at Kaʻala and ParkHQ. At all sites except for Laupāhoehoe, CWI comprised a significant part of the local water budget, especially at ParkHQ where the annual potential evaporation was nearly equal to RF (Figure 11).

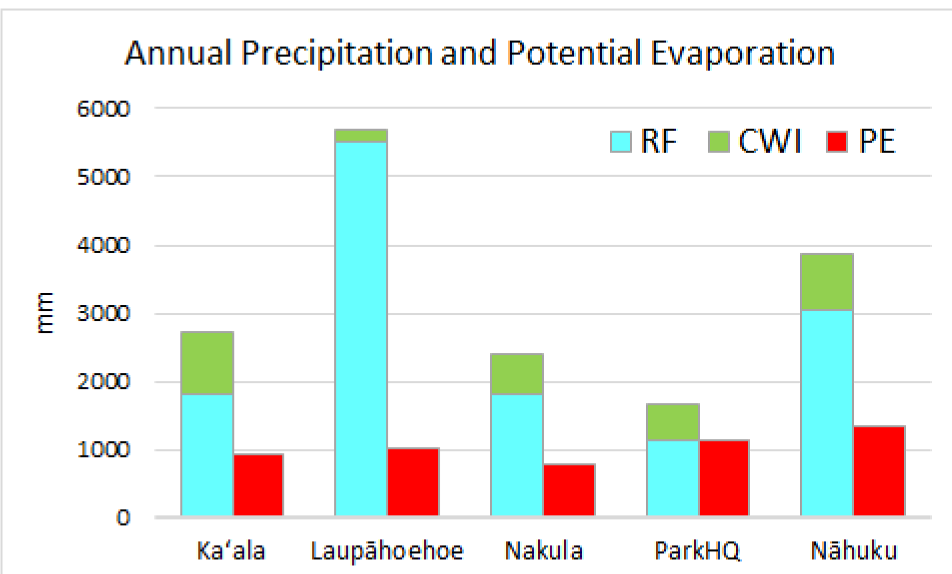

Figure 11. Mean annual precipitation, including rainfall (RF) and cloud water interception (CWI), and potential evaporation (PE), at each field site.

Fog frequency at Ka'ala was about 3 times as high as rain frequency, while at the other sites fog was about the same or less frequent than rain (Figure 12). However, CWI was more frequently detected than fog at all sites other than Ka'ala, especially at Nakula.

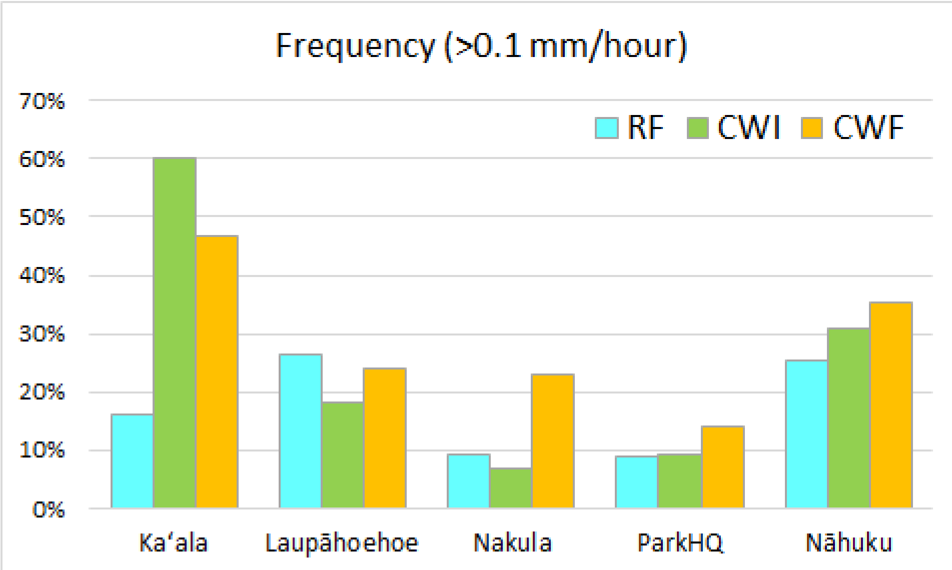

Figure 12. Occurrence frequency of rainfall (RF), cloud water interception (CWI), and fog (denoted by CWF), defined as the percentage of hours during the study period when the measured or estimated hourly RF, CWI, and CWF, respectively, exceed 0.01 mm per hour.

Field observations: Diurnal cycle and seasonal patterns

At all sites, RF reached its maximum in the afternoon, and higher RF values continued into nighttime hours at Nāhuku and Laupāhoehoe (Figure 13). The CWI diurnal cycles were relatively consistent among sites and similar to that of RF, with the only exception found at Nāhuku. Two general patterns were observed for the CWF diurnal cycles, where CWF was high during nighttime at Ka'ala and Nāhuku while at other sites the CWF roughly followed the RF pattern. LWC only exhibited a clear diurnal trend at Ka'ala with the maximum occurring in the afternoon. This high LWC during RF maximum may be the result of very small raindrops present in light drizzle mixed with cloud droplets and are difficult to separate by the wind-driven rain error correction. We found a clear wind direction cycle at Nakula which showed the change from southeastern land breeze to northwestern sea breeze in the mid-morning and the opposite after sunset. The diurnal wind direction change was closely related to the patterns of rainfall and fog because the moisture from the ocean brought by upslope wind is a primary cause of cloud formation at Nakula (Figure 13). A similar diurnal pattern was observed at ParkHQ where wind direction changed from east to west during the late morning through afternoon.

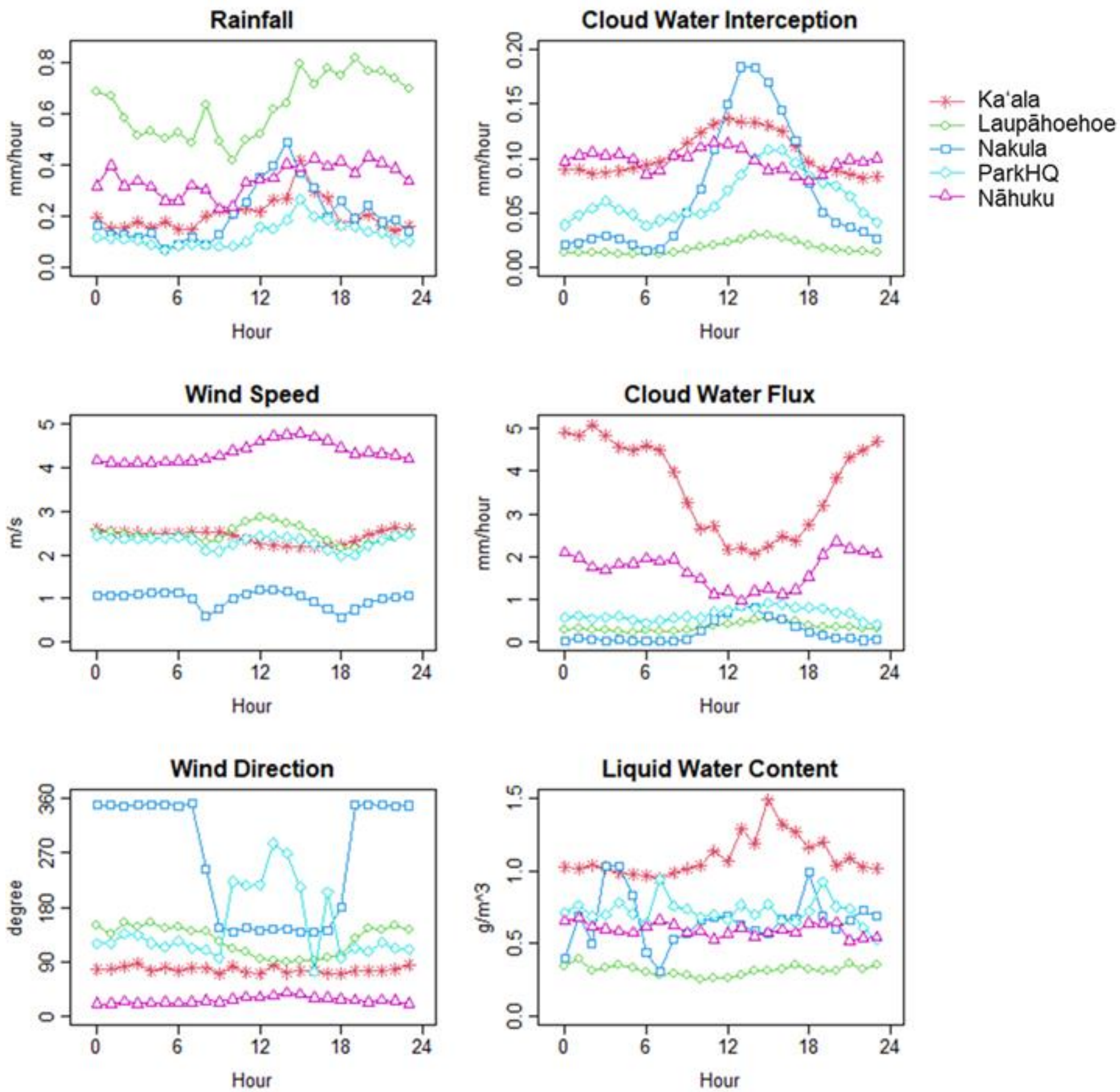

Figure 13. The mean diurnal cycle of selected variables at all sites. Wind directions are shown in degrees where 0 and 360 = North, 90 = East, 180 = South, and 270 = West.

While the data may not represent the general seasonal trends at these sites due to the short study periods, some patterns can be observed. The winter months are generally wetter with higher monthly RF, CWF, and CWI, and somewhat higher LWC during fog events (Figure 14). A different pattern was found for Nakula where CWF appeared to be higher in the summer months when RF was at its lowest. This may be the effect of stronger thermal convection and sea breeze in summer due to the increased heating of the land mass.

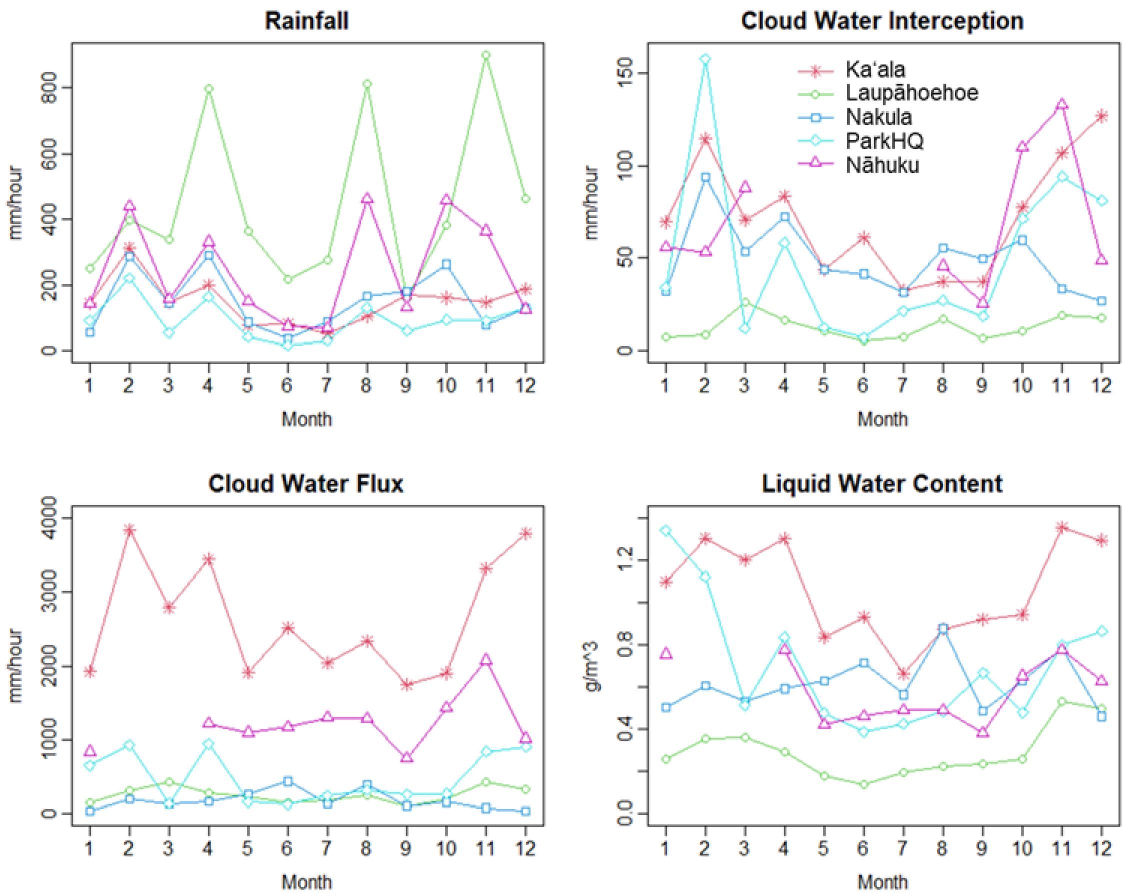

Figure 14. Mean monthly values of rainfall (RF), cloud water flux at canopy height (CWF_h), liquid water content during fog events (LWC), cloud water interception (CWI), horizontal wind speed (WS), and wind direction (WD). Monthly values with more than 80% of the data missing are not shown. Months are denoted as 1-12, corresponding with January-December 2017.

Testing the CWI empirical model

The linear regression results yielded moderate correlation between CWI and CWF, with R^2 of 0.37 – 0.59, and values of canopy interception rate (A) estimated by the slope of the fitted line varied from 0.014 to 0.064 across sites, indicating the variability of interception rates across sites with different vegetation types (Figure 15; Row 1 in Appendix O, Table 1).

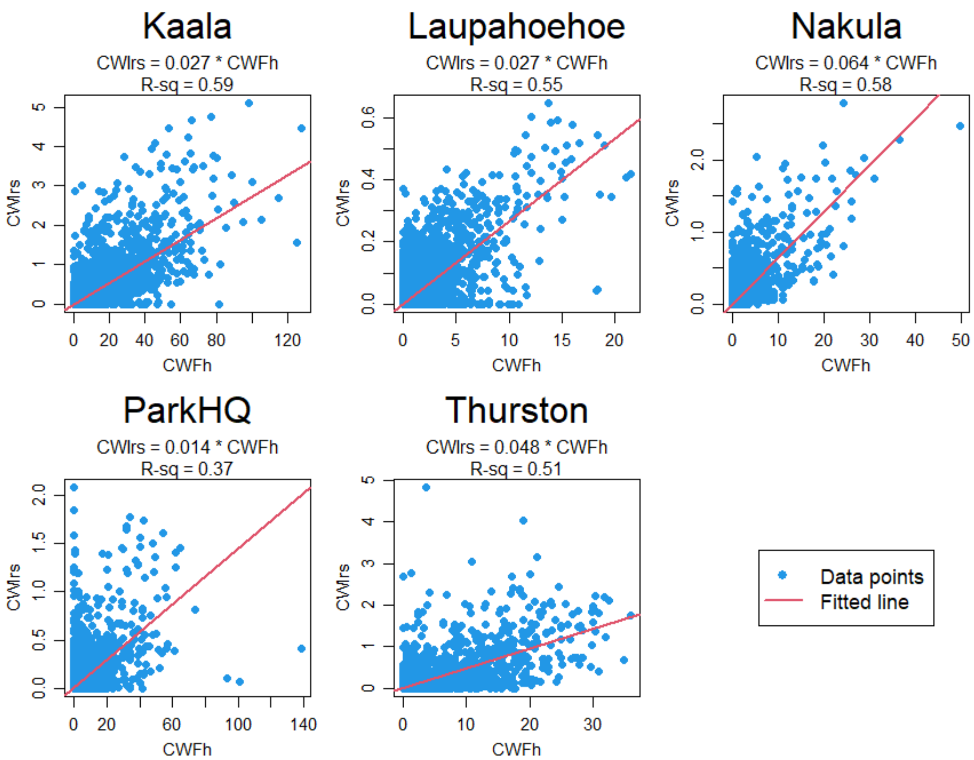

Figure 15. Linear regression between the hourly values of cloud water interception per ground area (CWI_{rs}) and cloud water flux at canopy height (CWF_h).

We fitted a linear and a nonlinear model to predict the canopy interception rate (A) by canopy height and leaf area index (LAI). The fitted model parameters were relatively close to the original model in Katata et al. (2011), but the original model tended to predict a higher interception rate than our models (Figure 16; Appendix O). The nonlinearly fitted model had the lowest prediction errors (root-mean-square error, RMSE).

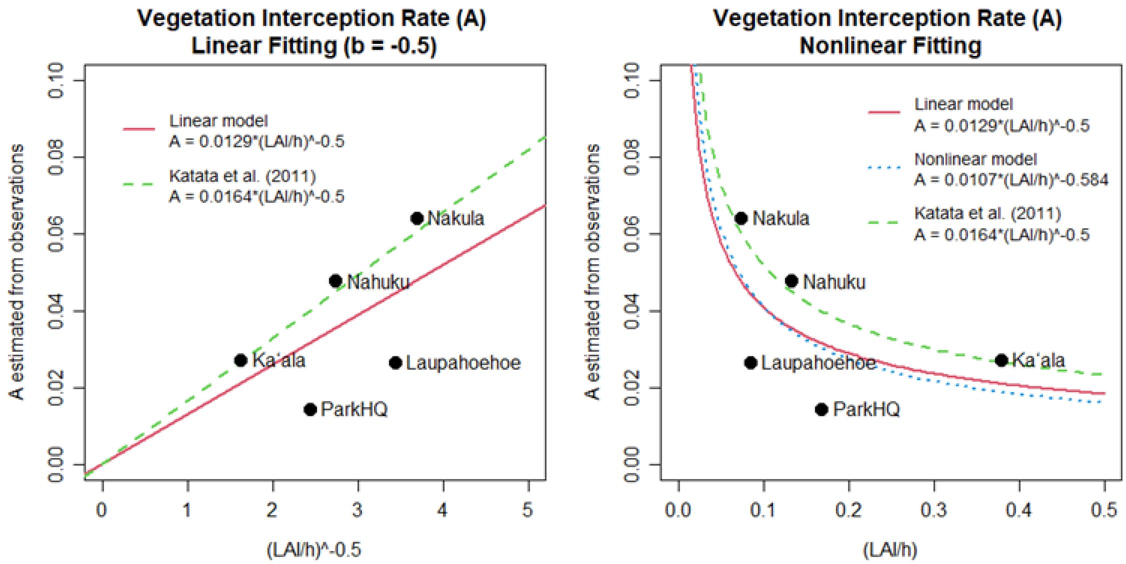

Figure 16. Vegetation interception rate (A) observed at five sites (dots) compared to A predicted by the original and the fitted models (solid and dashed lines) based on canopy height (h) and leaf area index (LAI).

We tested all three models by predicting cloud water interception per ground area from CWF observations at each site. Figure 17 compares the CWI predicted by each model to the observed cloud water interception per ground area and CWF.

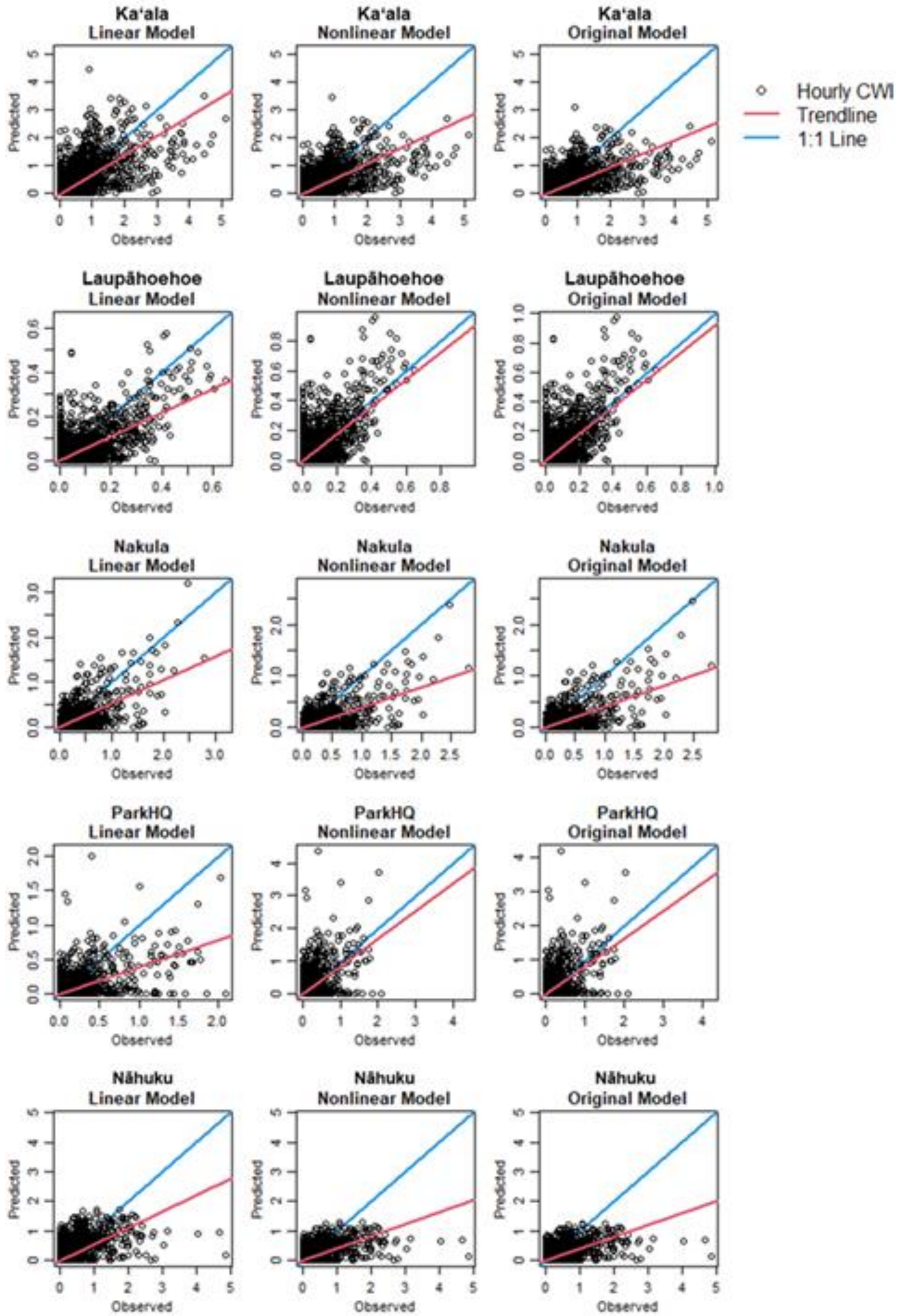

Figure 17. Comparison of observations (x-axis) to model predictions (y-axis) of hourly cloud water interception (CWI) at five sites. Each row shows results for one site and each column shows predictions made by different models (from left to right): linear-fitted model, nonlinear-fitted model and original model (Katata et al. 2011).

Model performance was assessed by the percent difference of the annualized CWI predictions to the observations and RMSE. RMSE is in the same units as the hourly CWI values and represents the error in hourly CWI predictions (Table 4). For easier comparisons between sites that have different levels of CWI, RMSE was normalized by the mean hourly CWI at individual sites (relative RMSE). When averaged across all five sites, the linear model underestimated annual CWI by 17% with a relative RMSE of 3.63; the nonlinear model underestimated annual CWI by 19% with a relative RMSE of 3.60. The original model overestimated annual CWI by only 6% but had the largest relative RMSE of 4.08 among all models. Although RMSE values seem high (e.g. a relative RMSE of 3 means the average prediction error is 3 times the mean CWI value), associated errors caused relatively small effects to the absolute amount of predicted CWI.

The original Katata model tended to predict a higher interception rate than the fitted model (Figure 16; Appendix O, Table 1). Because CWI predictions are proportional to interception rate, this caused the original model to predict a larger value for each hourly CWI. Although this led to higher annual CWI amounts that matched closer to the observations, the higher RMSE indicated that the overall differences in each pair of observed and predicted hourly CWI was greater than the other models.

The site with the largest errors was Nakula, where CWI was underestimated by more than 50% across all models (Table 4). We believe there are two sources of error for this site, both related to the patchy vegetation. CWI observations were based on measurements taken within a small isolated, exposed remnant stand of trees surrounded by shorter vegetation. Because of the small patch size and its exposure to wind-driven fog, we assume that fog capture is enhanced relative to sites within continuous forest. This edge effect is known to produce high rates of CWI (Giambelluca and Gerold 2011) and suggests that our model is likely to underestimate CWI in areas with isolated patches of tall vegetation. In addition to the enhanced CWI, the stand at Nakula was also affected by wind-driven rainfall. Rainfall striking the upwind edge of the patch can concentrate rainfall interception, causing the received rainfall to be locally higher than that indicated by the rain gauge. The enhanced rainfall capture would be falsely attributed to CWI by the SLWCWB model, causing the CWI observations to be overestimated. Hence, some of the model error observed for Nakula may be due to error in field-based estimates of CWI.

Table 4. Model predictions of annualized cloud water interception (Est.) and prediction errors measured by percent difference (%Diff, negative values denote underestimation) to the observed cloud water interception per ground area (CWI_{rs}) and the root-mean-square error relative to mean hourly CWI at each site (RMSE).

Site	Observations		CWI predicted by CWF & interception rate				
				CWI estimated by:			
	CWI_{rs}	CWF_h		CWI_{rs} vs CWF regression	Katata et al. (2011)	Linear fitted model	Nonlinear fitted model
Ka‘ala	911	41373	Est.	1123	1103	871	782
			% Diff.	23.3%	21.1%	-4.4%	-14.1%
			RMSE	2.17	2.16	2.12	2.15
Laupāhoehoe	158	3485	Est.	93	196	155	158
			% Diff.	-41.3%	24.3%	-1.8%	0.0%
			RMSE	3.04	4.29	3.62	3.66
Nakula	299	2192	Est.	140	132	105	108
			% Diff.	-53.1%	-55.7%	-65.0%	-63.9%
			RMSE	3.21	3.21	3.29	3.28
ParkHQ	158	6302	Est.	91	252	199	191
			% Diff.	-42.7%	59.1%	25.6%	20.8%
			RMSE	4.72	8.31	6.60	6.38
Nāhuku	860	15121	Est.	720	679	536	526
			% Diff.	-16.2%	-21.0%	-37.6%	-38.8%
			RMSE	2.44	2.45	2.53	2.54

2) Ecological responses to fog immersion and CWI

Fog effects on transpiration

Weather conditions at Nakula lacked clear seasonality during the study period of September 2016 - December 2017 (Figure 18). We found decreasing trends in soil moisture in 2016 and 2017 during rainless periods, although a clear decreasing trend was not observed in transpiration during these periods. Vapor pressure deficit (VPD), which indicates the dryness of the atmosphere and drives transpiration, was calculated from relative humidity and air temperature data collected at each site. VPD fluctuated diurnally and often showed high values even at nighttime (Figure 19). Daytime VPD increased with decreasing relative humidity and increasing air temperature (drier, warmer conditions), while high nighttime VPD was due to decreased relative humidity rather than increased air temperature.

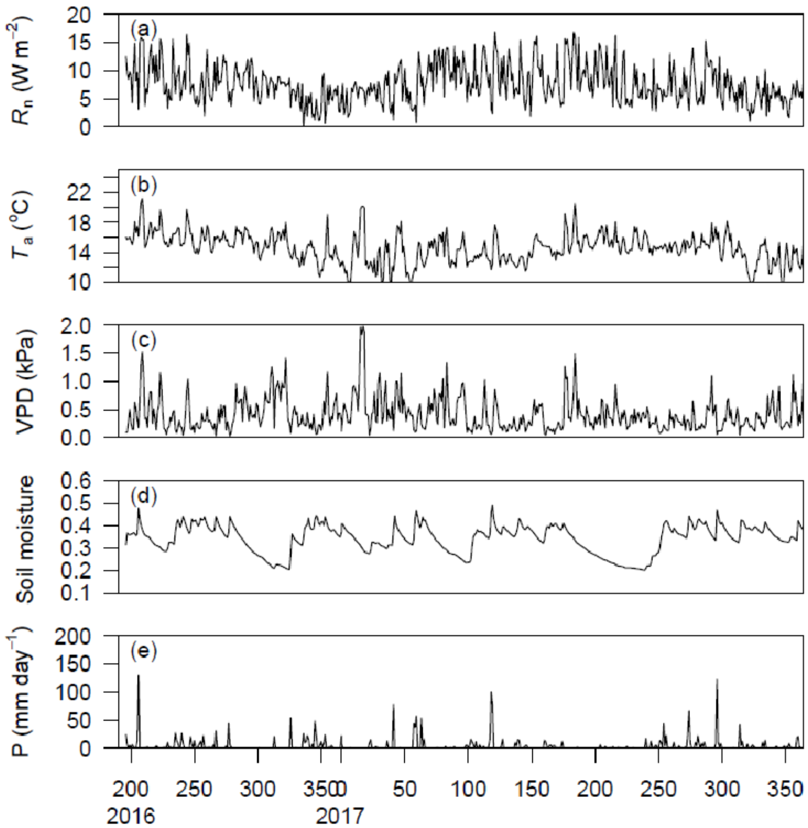

Figure 18. Weather conditions for the Nakula site include: (a) net solar radiation (R_n), (b) air temperature (T_a), (c) atmospheric vapor pressure deficit (VPD), (d) soil moisture and (e) rainfall (P) during September 2016 - December 2017.

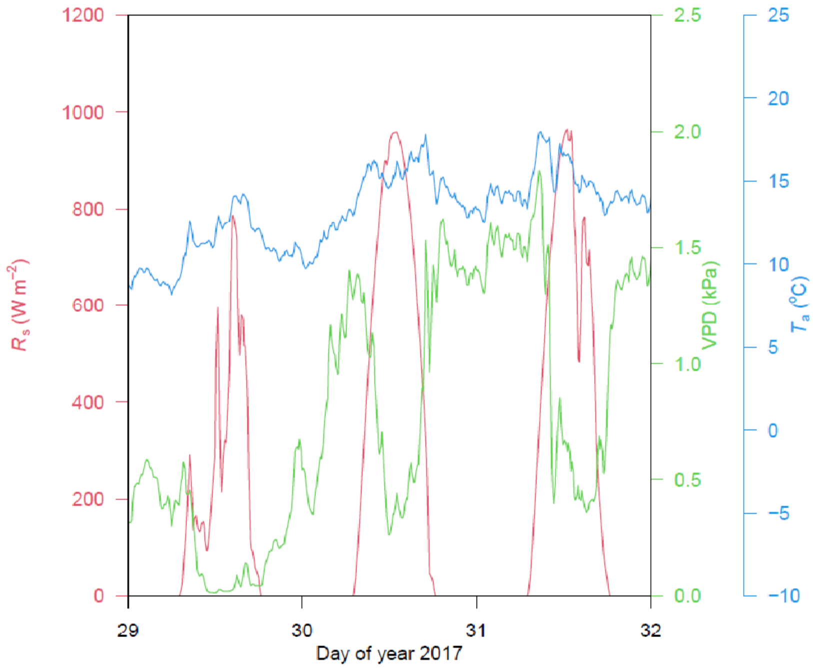

Figure 19. Weather data at 10-minute intervals for net solar radiation (red), air temperature (blue) and atmospheric vapor pressure deficit (VPD; green) from day of year 29 until 32 in 2017.

At night, trees exhibited a strong relationship between heat pulse velocity (HPV, a measure of transpiration rates, hereafter 'transpiration') and VPD, without clearly levelling-off at high values of VPD. High rates of transpiration were observed under high VPD, while transpiration rates were low during wet conditions when VPD was also low. In daytime, the HPV-VPD relationship varied under different light intensities (Appendix P). Under each light intensity, transpiration rates increased with increasing VPD at VPD below 0.5-1 kPa, but the upper envelope of the relationship showed a levelling-off at higher VPD. Trees exhibited higher rates of transpiration under higher net solar radiation (incoming solar radiation minus reflected solar radiation) than under lower net solar radiation both at high VPD and low VPD ranges, suggesting solar radiation energy input enhances transpiration (Jarvis and McNaughton 1986) and/or increased stomatal conductance for photosynthesis in response to the increased net solar radiation (Dang et al. 1998).

Environmental controls on plant growth and seedling recruitment

Tree diameter fluctuations to understand controls on growth

‘Ōhi‘a and koa trees showed strong variation in stem diameter due to bark wetting and peeling effects. These complicating effects were minor for the smaller ‘a‘ali‘i, which showed strong steady growth alongside diurnal variation (Figure 20).

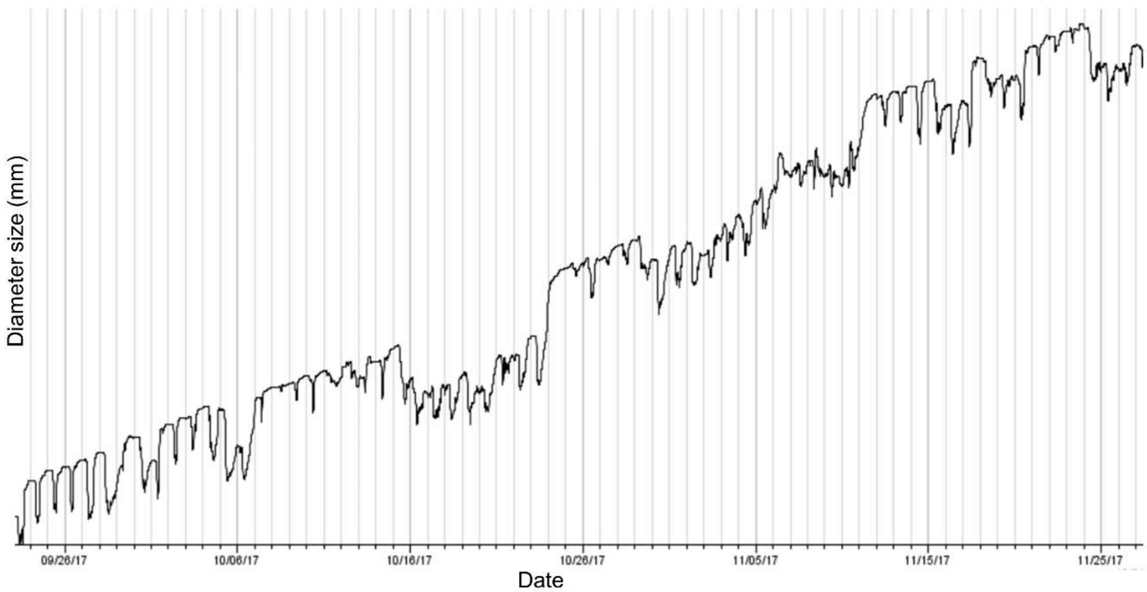

Figure 20. Example of daily diameter change for ‘a‘ali‘i individual during September 2016 - November 2017.

Controls on daily ‘a‘ali‘i diameter growth (occurrence)

We focused on relating ‘a‘ali‘i stem diameter to climate data sets to identify the drivers of plant growth at Nakula and found a strong pattern of moisture dependence (Figure 21).

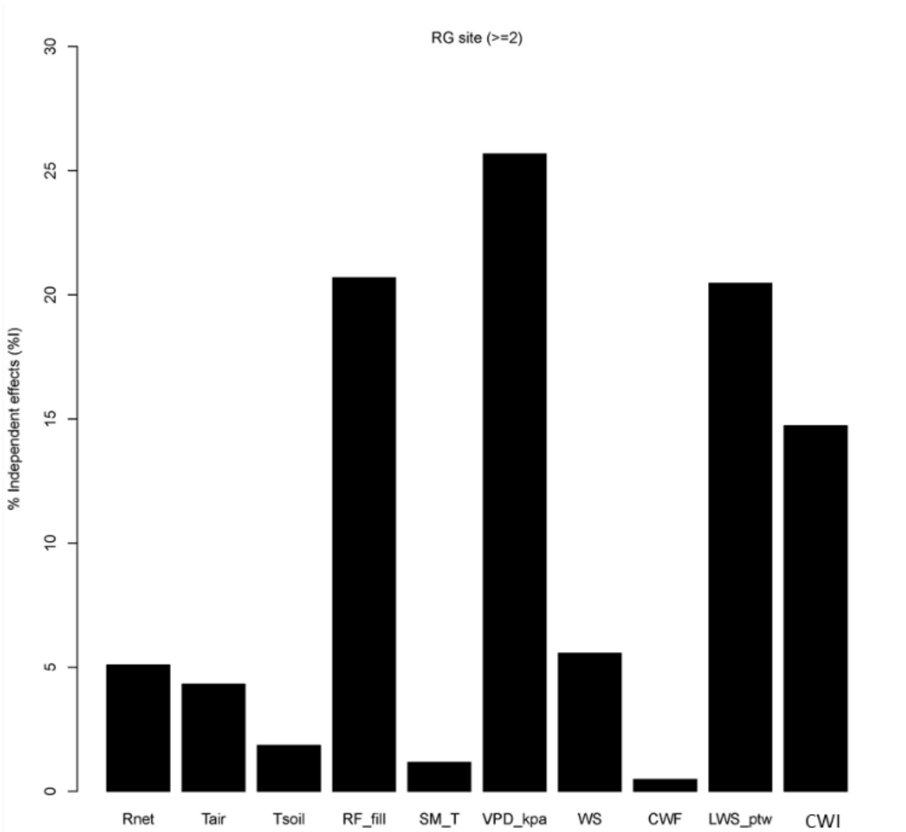

Figure 21. Hierarchical partitioning of variance illustrating the strong contribution of rainfall (RF_fill), vapor pressure deficit (VPD_kpa), proportion of time when leaves are wet (LWS_ptw), and cloud water interception (CWI) to daily ʻaʻaliʻi stem diameter changes.

The logistic regression model selection exercise yielded numerous comparable "best" models (Appendix Q). The consistent emergence and sign of rainfall (RF) and VPD variables across the model selection and hierarchical partitioning exercise support the interpretation of ʻaʻaliʻi daily RG as moisture-dependent. Unexpectedly, wind speed also emerged as a strong predictor (negative effect) while cloud water interception (CWI) did not. Leaf wetness and soil moisture had secondary importance, with leaf wetness having a positive contribution to growth while soil moisture having a negative effect, which is counterintuitive and warrants further examination. Calculation of variance inflation factors confirmed that the models did not include any collinear predictors.

Comparing binomial ʻaʻaliʻi real growth to days classified by precipitation type (clear, fog-only, rain-only, and rain+fog, derived from classification of different precipitation events), we found that days of precipitation, especially rain+fog days, were associated with the occurrence of real growth while most days when no real growth occurred were associated with clear conditions (Table 5, $\chi^2_{(3, 679)}$ = 179.94, p<0.001)

Table 5. Contingency table comparing ‘a‘ali‘i tree growth response and days classified by precipitation conditions during March 2016 – March 2019 when data were available for a 24-hour period. Values indicate observations; values in parentheses indicate expected value. Growth was strongly associated with precipitation. Differences were significant at the 0.05 level (*n* = 679, $\chi^2_{(3, 679)} = 179.94$, $p<0.001$).

	Clear	**Fog only**[1]	**Rain only**[1]	**Rain + fog**[2]	Total
Real growth observed (expected)	104 (179)	75 (68)	39 (36)	258 (193)	476
No real growth observed (expected)	151 (76)	22 (29)	12 (15)	18 (83)	203
Total	255	97	51	276	679

[1] *defined by any instance of fog or rain*

[2] *defined by any combination of fog and rain*

Controls on weekly ‘a‘ali‘i, ‘ōhi‘a, and koa diameter growth (RG)

In addition to looking at daily binomial growth responses, we examined the total weekly increase in stem diameter of vigorously growing ‘a‘ali‘i and established ‘ōhi‘a and koa trees at Nakula. Species differed in the relative magnitudes of growth and there was no obvious seasonality to the growth of the species (Figure 22).

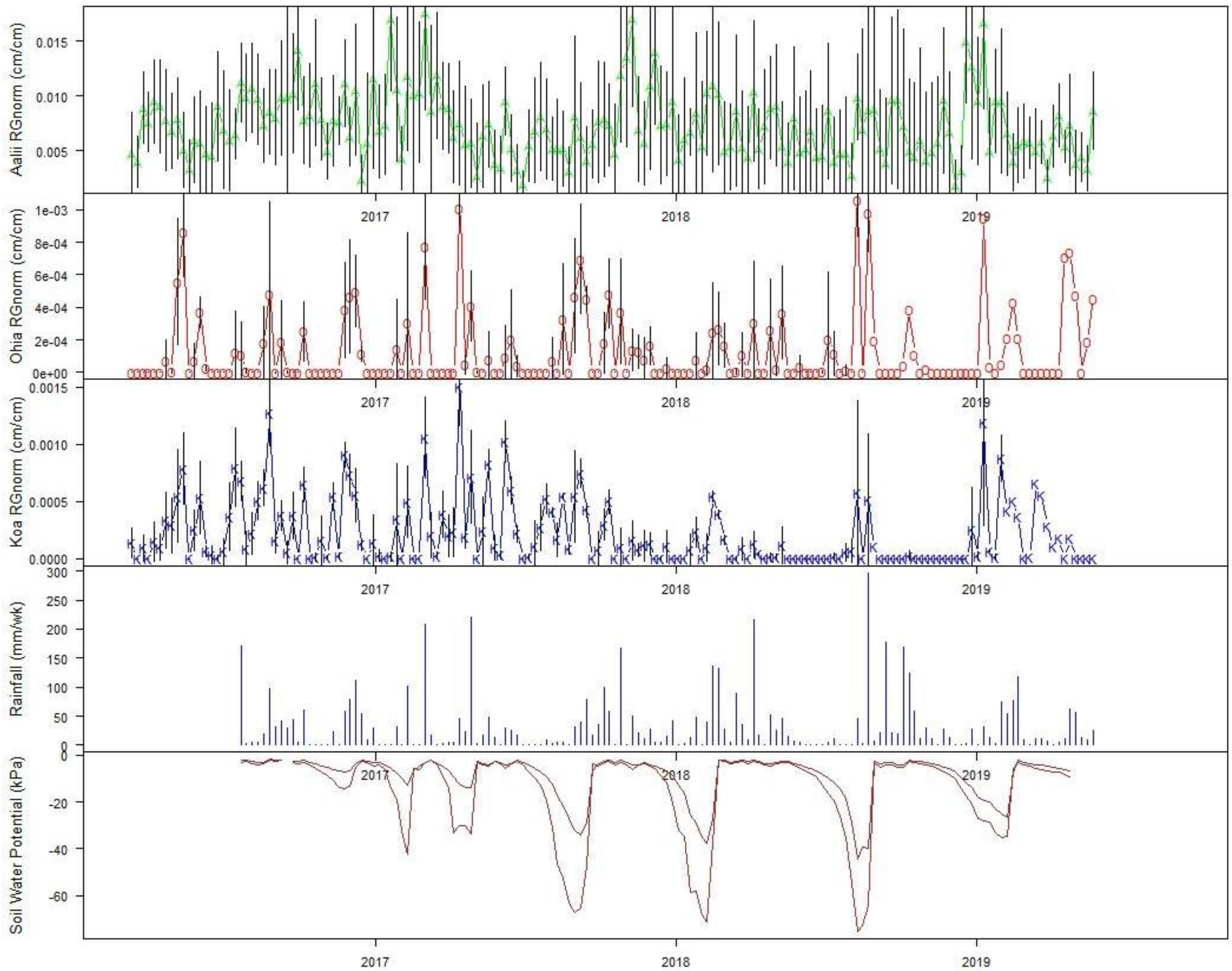

Figure 22. Weekly growth (scaled RG) by species: ‘a‘ali‘i, ‘ōhi‘a, koa means and standard deviation (bars), weekly rainfall, and soil water potential at 88 and 119 cm depth in a koa grove (site R19).

We found that different variables emerged as important for explaining each species' weekly growth (Appendix R). ‘A‘ali‘i weekly growth was positively associated with higher rainfall, lower leaf wetness and net radiation. ‘Ōhi‘a and koa weekly growth were also positively associated with rainfall as well as cloud water flux. Interestingly, koa weekly growth was also explained by wind speed (positive effect) as well as VPD and soil moisture (negative effects). Additional covariates important for explaining ‘ōhi‘a weekly growth included leaf wetness which positively influenced growth, while net radiation and VPD had negative effects on growth.

Controls on weekly ‘a‘ali‘i, ‘ōhi‘a, and koa diameter water deficit (WD)

Water deficit, as the difference between measured diameter and the growth line, tended to be more synchronous across species than real growth. Water deficit responded more immediately to environmental conditions affecting plant water status and was a relatively less noisy measurement for the big trees of ‘ōhi‘a and koa (Figure 23).

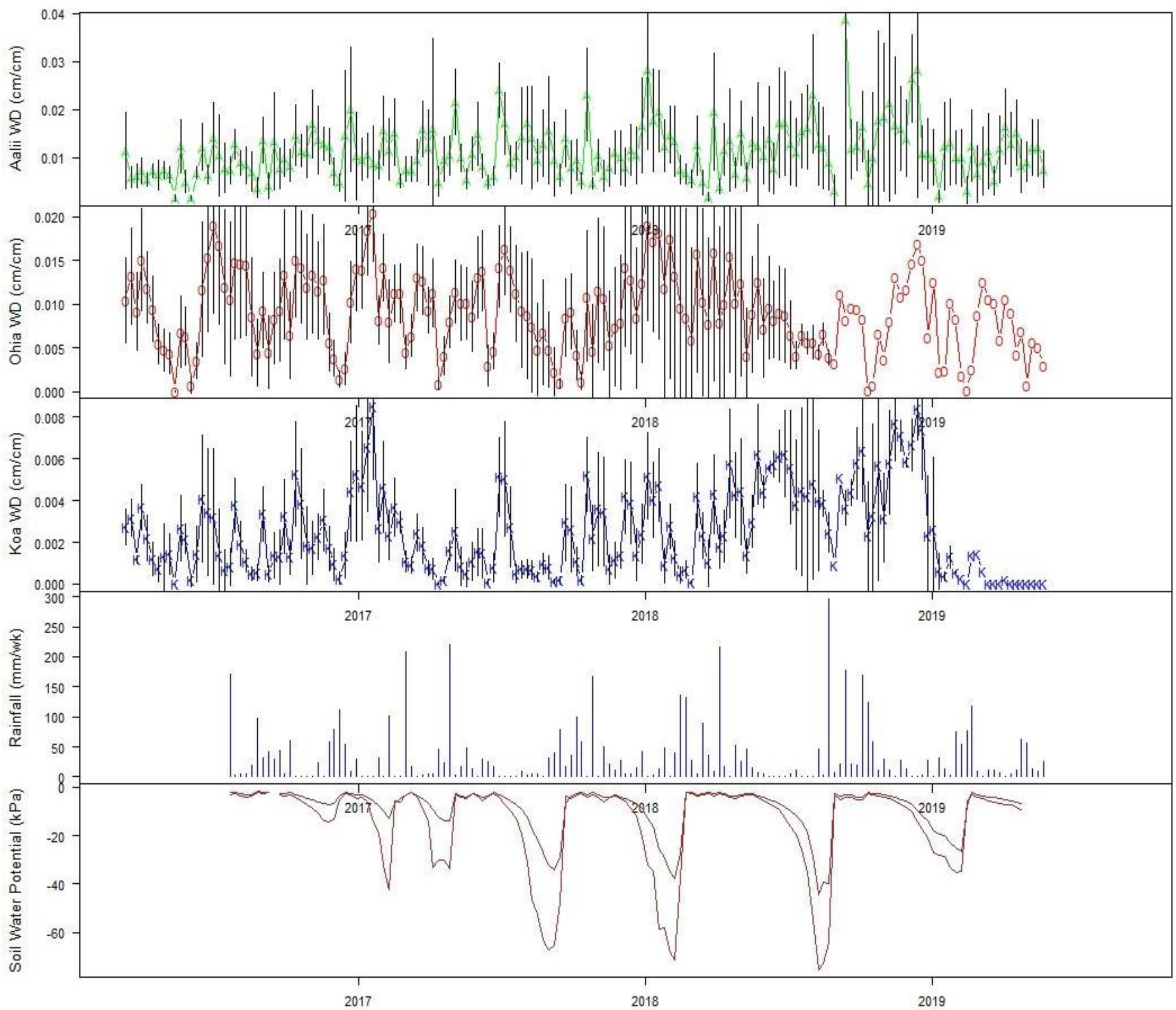

Figure 23. Weekly water deficit (scaled WD) by species: ‘a‘ali‘i, ‘ōhi‘a, koa and weekly rainfall and soil water potential at 88 and 119 cm depth in koa grove (site R19).

Using linear regression and multimodel selection, we found that higher vapor pressure deficit periods were associated with higher plant water deficits for all species (Appendix S). The relative importance of other environmental variables to the species water deficits, however, was less consistent. ‘A‘ali‘i water deficits appear to be reduced with cloud water flux and exacerbated by higher net radiation, and for ‘ōhi‘a, higher temperatures appeared to reduce water deficit, although this warrants further examination. The ‘ōhi‘a data were particularly noisy and the WD metric was sensitive to errors associated with bark peeling. The results from the koa WD models were counterintuitive and also warrant further examination as the results suggest higher soil moisture exacerbated koa water deficit while higher net radiation ameliorated it.

Grass removal effects on soil moisture and response to precipitation

Grass removal had no effect on volumetric water content at 20 cm below the soil surface (Appendix T). Mean 20 cm soil moisture values for grass and no-grass plots were nearly indistinguishable, even during the early months of the study when we expected effects of grass removal to be strongest prior to its regrowth.

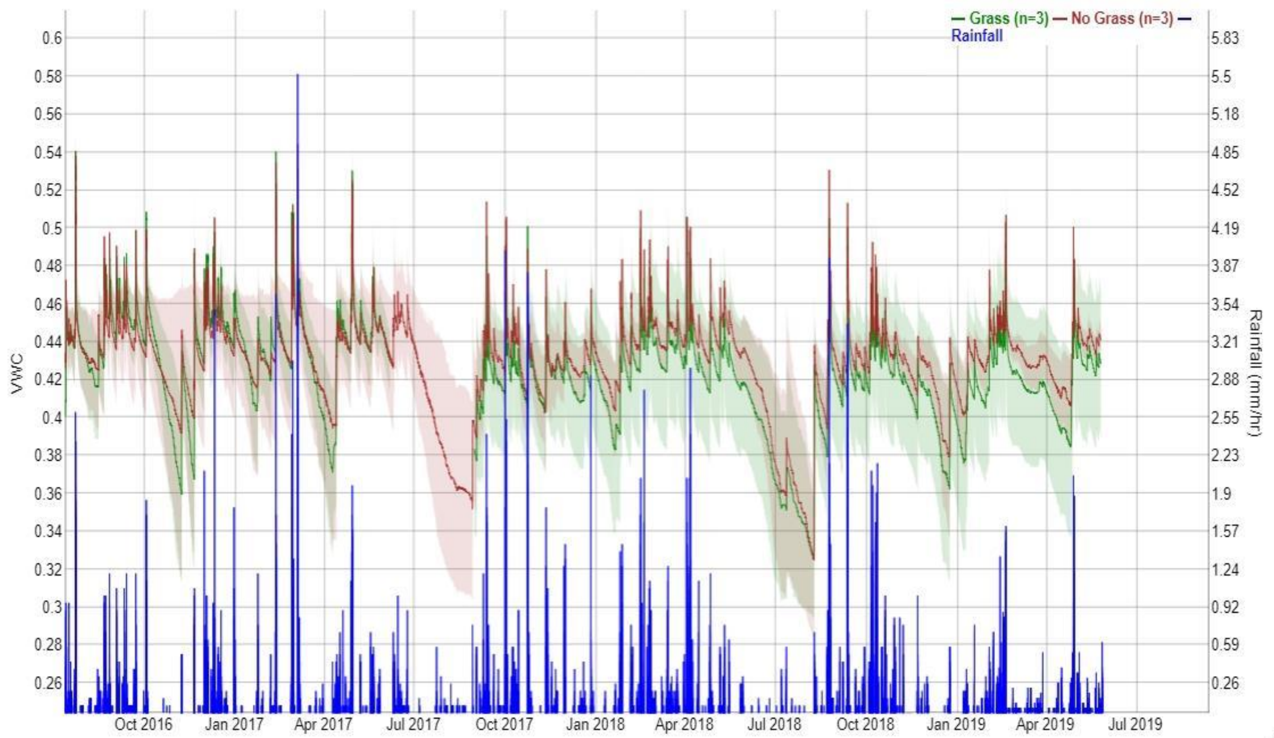

Figure 24. Soil moisture at 20-cm depth as volumetric water content (m^3m^{-3}) in grass control plots (green) and grass removal plots (brown). Mean soil moisture values were calculated from three sensors and shading represents standard deviation. The absence of shading indicates a period of sensor failure (n≤2, standard deviation is unavailable).

Although suffering from low statistical power (n=3) and later sensor failure, our results for 5 cm soil moisture during year 1 suggest volumetric water content is occasionally higher when grass is removed. The difference in soil moisture between the treatments was largest and marginally significant at the end of a long dry-down event in late 2016 (Figure 25).

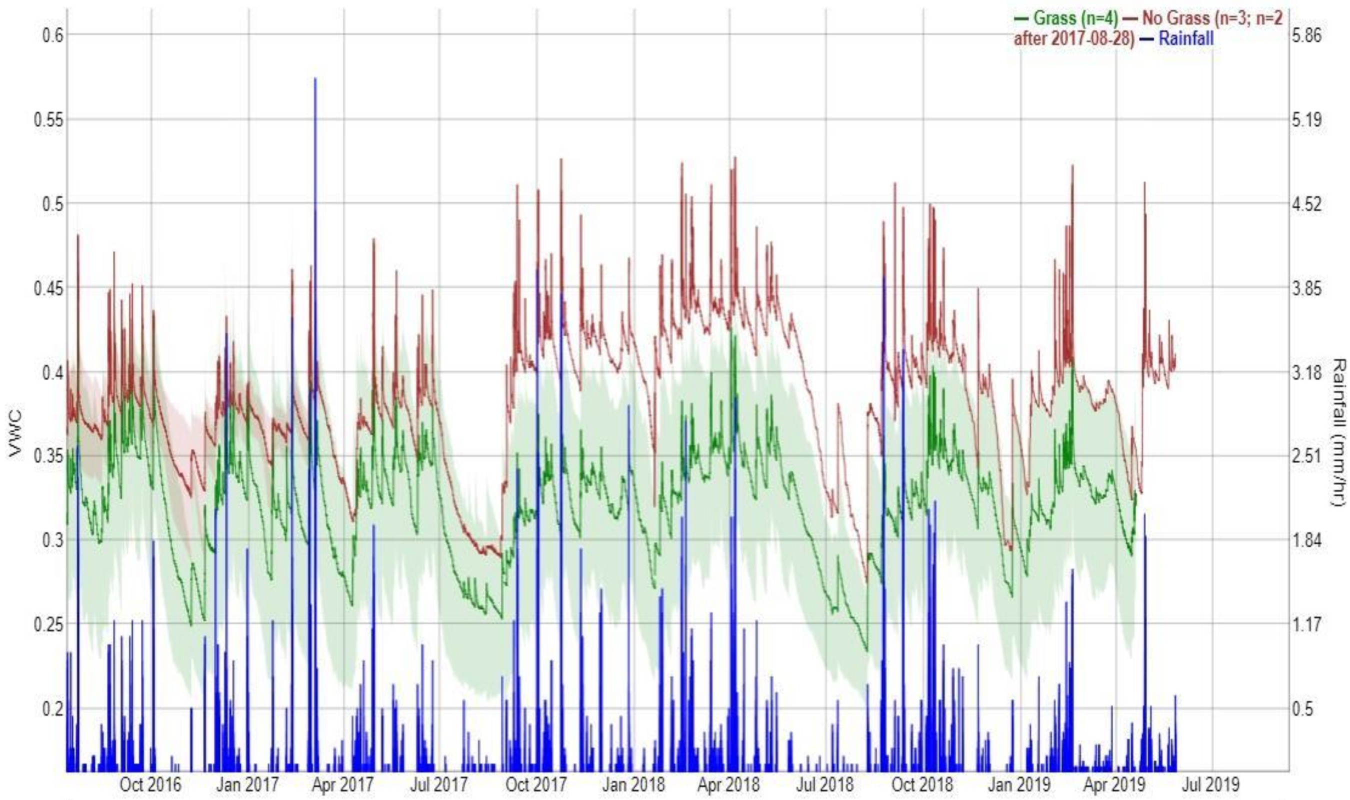

Figure 25. Soil moisture at 5-cm depth as volumetric water content (m^3m^{-3}) in grass control plots (green) and grass removal plots (brown). Mean soil moisture values were calculated from three sensors and shading represents standard deviation. In late August 2017, one of the no-grass plot sensors failed; we present the mean of the remaining two sensors, but standard deviation is unavailable.

To better understand the effect of fog and rainfall on soil moisture responses, we condensed 5 cm soil moisture data into mean daily responses (increase/decrease) and compared these to days classified by precipitation type (clear/fog only/rain only/rain + fog, see Table 6). The occurrence of different precipitation conditions had a strong effect on whether soil moisture increased or decreased with grass ($\chi^2_{(3, 89)}$ = 44.31, p<0.001) or under grass removal ($\chi^2_{(3, 88)}$ = 37.89, p<0.001).

Table 6. Contingency table of soil moisture (SM) responses to days classified by the occurrence of different precipitation types. Differences were significant at the 0.05-level (n = 89, 88; $\chi^2_{(3, 88)} = 37.89$; p<0.001).

Grass, 5 cm	clear	fog only	rain only	rain+fog	total
SM decrease	32	10	3	12	57
SM increase	1	0	1	30	32
total	33	10	4	42	89
No Grass, 5 cm	clear	fog only	rain only	rain+fog	total
SM decrease	31	9	3	13	56
SM increase	1	1	1	29	32
total	32	10	4	42	88

To explicitly test whether grass removal affected responsiveness of surface soils to precipitation events, we identified days when 5 cm soil moisture increased or decreased, grouping observations from grass/no grass plots and compared these to days classified by precipitation type. Grass removal treatment had no effect on daily mean 5 cm soil moisture responses across precipitation types whether we analyzed days of increase ($\chi^2_{(3, 64)} = 0.10$, p=.99) or decrease ($\chi^2_{(3, 113)} = 1.02$, p = .797).

Grass removal effects on seedling recruitment

‘A‘ali‘i seedlings showed a pulse of recruitment after plots were cleared of grass biomass (Figure 27), but as exotic grasses filled back in, there were few new seedlings. We never found seedlings in the control plots where grass remained intact. Most seedling death took place within the first several months after monitoring began and then leveled off. The three separate sites showed variability in overall number of seedlings germinating by the end of the experiment, as well as mortality patterns. For example, Spray 6 showed a sharp mortality event in the smallest size class of ‘a‘ali‘i in late 2016 that also led to an overall decrease in total ‘a‘ali‘i seedlings (Figure 26). This time period coincided with a long dry-down period (Figure 25). In contrast, while 0-5 cm seedling counts decreased during this time in Spray 2, total seedling numbers still increased overall, and ‘a‘ali‘i seedling counts in Spray 4 did not decrease at this time in any size class.

Of the individually tracked seedlings (30 per site), survival averaged 54.4% across sites by the end of the study, although there was large variation by site (Figure 27). There was no relationship between a seedling being surrounded by/covered by exotic grass and the probability of survival. Even as grasses filled in, seedling survivorship remained high

(Figure 27). This suggests that once seedlings reach a large enough size, they are less likely to die, even in 100% exotic grass cover.

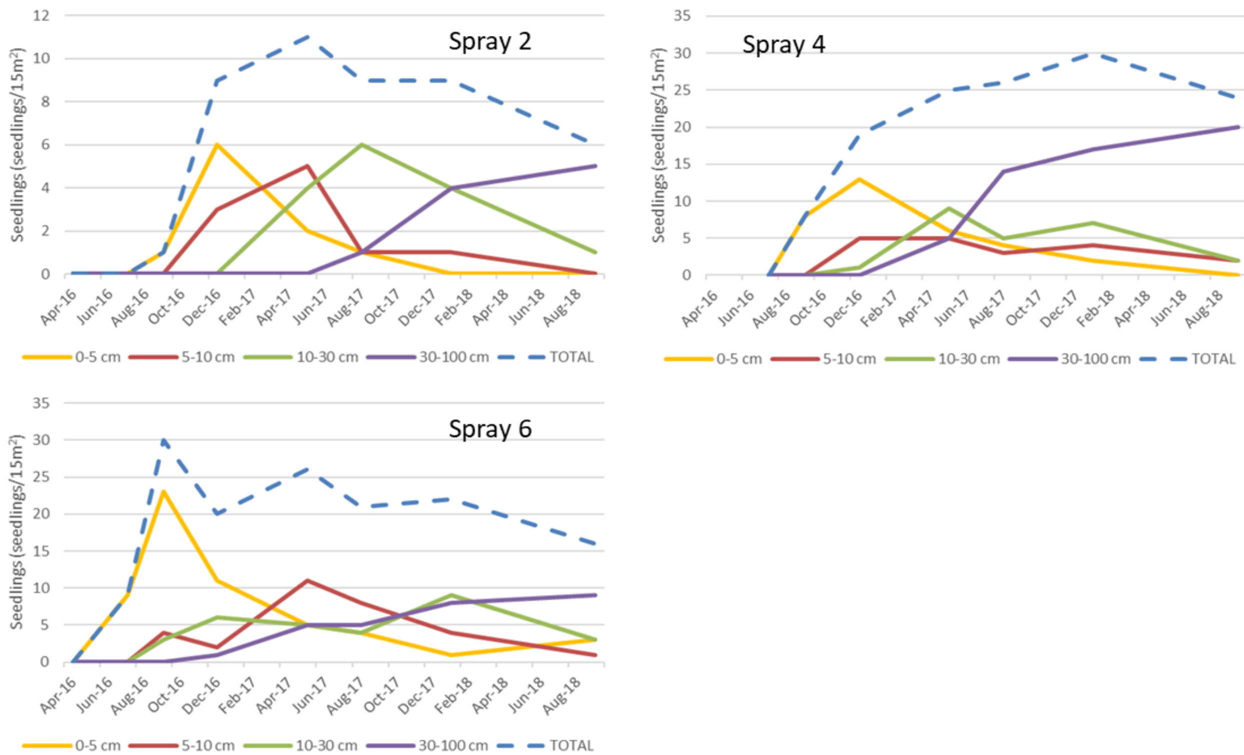

Figure 26. Counts of ‘a‘ali‘i seedlings in different height size classes (0-5 cm, 5-10 cm, 10-30 cm, and 30-100 cm tall) as well as a cumulative total in three different sites, from April 2016 - August 2018.

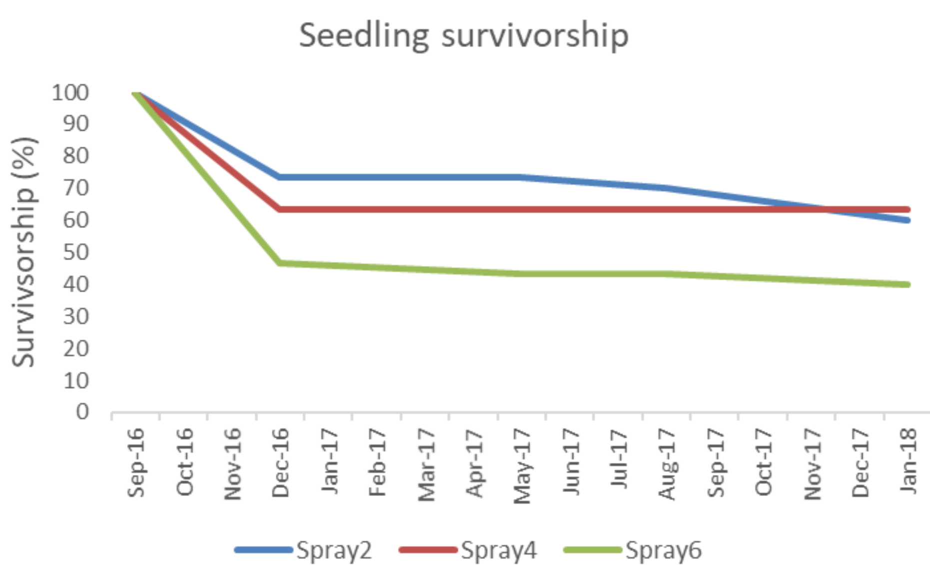

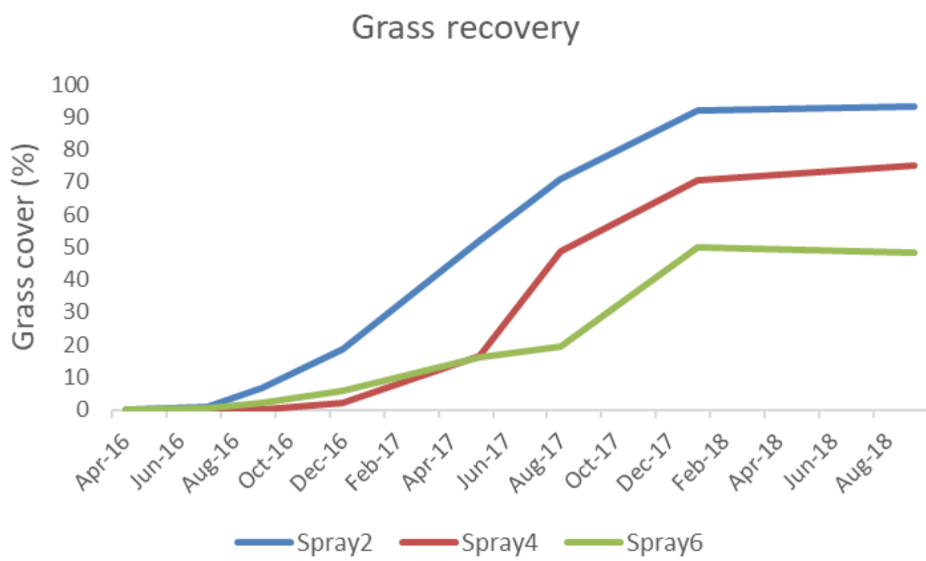

Figure 27. Individual ʻaʻaliʻi seedling survivorship (top) and exotic grass cover (bottom) in three different sites from June 2016 - August 2018. Note that survivorship levels off (no further mortality) even after grass attains 100% cover.

3) Soil moisture monitoring to link CWI with drought

The soil moisture measurements collected during the data-collection program were summarized in a USGS data release by Kennedy et al. (2019). The data release includes a summary file, three results files, and one metadata file. The summary file includes tables and maps that describe the locations and dominant vegetation for each of the three CWI study sites. Two results files include a tabular summary of soil particle-size, dry bulk density, porosity, volumetric water content, and gravimetric water content analyses made on soil samples collected at three study sites between July 2016 and July 2017. The third results file includes a summary of measurements of soil field-saturated hydraulic conductivity, hydrophobicity, and preferential flow collected at the Nakula site during January 2018.

vii. ANALYSIS AND FINDINGS:

1) CWI measurement and model

Field observations at five different locations confirmed that CWI is highly variable through space and time. The temporal changes in CWI were closely associated with changing atmospheric conditions that affect CWF (including wind speed), and the site differences were controlled both by CWF variation and vegetation types. Canopy height and LAI describe the vegetation's ability to convert cloud droplets moving over the land surface into a form of precipitation relatively well. However, at sites where the canopy is highly fragmented, canopy height and LAI alone may be insufficient to explain the enhanced interception rate due to increased wind exposure by isolated trees and at forest edges. We also note that in these fragmented landscapes, CWI estimates using field observations are subject to error associated with enhanced capture of wind-driven rain by small, isolated patches of trees.

No clear relationship was found between CWI and rainfall or elevation, suggesting CWI predictions based on elevation range and a fixed ratio to rainfall over-simplified the spatial and temporal variability and may introduce large biases. Instead, the CWI model developed by this project can be used to simulate large scale CWI patterns across Hawaiʻi wherever data is available, and more accurately than most previous works. The CWI model may also be used to conduct simulation experiments and predict potential impacts of climate change, species invasion, or restoration and ecosystem management practices on water budgets.

When properly calibrated, passive fog gauges can be a very useful tool for monitoring LWC and CWF at remote sites because of its low-cost and relative simplicity compared to commercial LWC sensors. Deploying fog gauges at multiple locations provided data crucial to characterizing the spatial variation of CWF.

The fog gauge calibration methods established in this project are readily available to be used in future studies. The calibration method can also be modified to calibrate other fog gauge types as long as an accurate LWC sensor is available for testing, and collocated rain rate and wind speed measurements could be made simultaneously. While fog gauges are among the most common methods used in TMCF and CWI studies, the gauge efficiency and WDR errors have largely prevented quantitative comparisons of different studies. Converting fog gauge measurements into LWC would greatly improve the comparability of TMCF studies across sites around the world.

2) Ecological responses to fog immersion and CWI

Fog effects on transpiration

We found that the leaf surface VPD was highly coupled to the atmospheric VPD at Nakula. We believe that atmospheric VPD well represented leaf surface VPD in this study site and that fog decreased both atmospheric and leaf surface VPD, which depressed transpiration.

The fog presence, and resultant decrease in VPD, contributed to decreased transpiration by koa at Nakula. Fog frequently occurred in daytime when the slope of HPV-VPD relationship was steepest, suggesting higher stomatal conductance (plant energy accumulation) in daytime than at nighttime (Phillips and Oren 1998) If fog disappearance coincides with increased solar radiation, transpiration may increase.

Nighttime transpiration

Nighttime transpiration increased with VPD rates for koa at Nakula, similar to findings reported for ʻōhiʻa (Gotsch et al. 2014). Because of the strong correlation between VPD and water use at nighttime, our results suggest that koa trees transpire at night rather than refilling water stores inside the tree body. Trees are known to close stomata in the dark (Dang et al. 1998) in order to avoid water loss during the photosynthetically non-productive period, but not always completely. Our results suggest that koa at Nakula do not fully close stomata at night, but largely reduce their conductance.

Nighttime transpiration accounted for a large part of transpiration in this study site. Transpiration from 18:00 until 6:00 was 35.5% of total daily transpiration during our study period in 2017. Small or zero transpiration at predawn was assumed in previous studies based on the lowered stomatal conductance in the dark and lowered VPD, which was not true in Nakula.

Environmental controls on plant diameter growth and water status

For ʻaʻaliʻi, the species with the lowest bark swelling effects, we found that precipitation (rain and fog) was positively associated with days of growth. Rainfall was an important predictor of weekly growth, and vapor pressure deficit was associated with greater stem water deficit. Interestingly, cloud water flux (fog) emerged as an important predictor of ʻaʻaliʻi water deficit, negatively affecting their values. This suggests that although cloud water flux might not contribute directly to soil moisture and plant growth, it likely reduces the degree of ʻaʻaliʻi stem shrinkage and maintains plant water status by reducing transpiration losses (Alvarado-Barrientos et al., 2014).

In contrast, the variation in stem diameter of the larger tree species appeared dominated by plant water status. However, stem diameter measurements were complicated by effects of bark swelling and peeling, making it difficult to identify clear patterns. More refined analyses focusing on smaller, specific periods of time may aid in discerning growth patterns from this tree dataset.

We observed differences between ʻaʻaliʻi sapling and mature ʻōhiʻa and koa tree stem diameter growth patterns likely related to rooting differences and depth of soil water uptake, where saplings are able to rapidly develop deep roots (Kulmatiski et al. 2010, Kulmatiski and Beard 2013). Baguskas et al. (2016) found that sapling water status benefited more from fog immersion than mature trees, likely because fog drip tends to influence soil moisture at shallow depths. Growth patterns in response to fog may also occur via ecosystem nutrient dynamics because fog events also affect soil microbial processes (Carbone et al. 2013), although this was not examined during the study.

Grass removal in a fog zone: effects on soil moisture and natural seedling recruitment

There was little difference in 5 cm soil moisture between plots with and without grass suggesting that the net effect of grass CWI and transpiration was somewhat equivalent to direct evaporation of moisture from bare soil. The amount of CWI due to interaction of fog with short and aerodynamically smooth vegetation such as grass is likely to be very low, consistent with observations of forest throughfall exceeding incident rainfall in a cloud-zone pasture in Kona, Hawaiʻi (Brauman et al. 2010). If grasses were able to capture enough moisture during fog events to make it into the soil surface, it was not enough to show a strong signal given these other processes. Over longer dry down periods, however, transpiration likely caused greater loss of soil moisture in grass control plots.

The main effect of grass on seedling recruitment and survival appears to be a bottleneck in recruitment in thick, undisturbed grassland. Because soil moisture did not vary between plots with and without grass, we posit that this result is primarily due to competition for light, rather than water. Once seedlings reached a certain size class in herbicide and grass removal sites, even being surrounded by grass regrowth did not lead to increased mortality. We note, however, that grasses at this stage, while present, were much thinner than the thick grass swards on the outside of the herbicided area. The average seedling survival for ʻaʻaliʻi in this study was high at 54.4%, suggesting that fog may still buffer harsh conditions (e.g., sunlight leading to higher plant transpiration and desiccation, direct evaporation from the soil). Similarly, MFBRP did not water seedlings during outplanting efforts at Nakula and recorded high survival in most species (80-90% survival: Warren et al. 2019), again suggesting that fog may play a buffering role given the site's aspect and rainfall.

viii. CONCLUSIONS AND RECOMMENDATIONS:

In this study, we developed linear and nonlinear models relating CWI to meteorological variables and vegetation canopy structure based on field observations. Moderate linear correlations were found between CWI and CWF observations made at five field sites. However, models underestimated CWI, especially for vegetation with isolated canopy fragments because the enhanced wind exposure was not represented in the model. Future research that includes additional vegetation structure metrics such as canopy openness may improve model predictions over these areas. For example, we expect that the short and continuous canopies at Kaʻala are less efficient in capturing cloud droplets while the isolated trees and forest edges, such as those at ParkHQ and Nakula, have better exposure to wind and CWF, while the taller canopies at Laupāhoehoe and Nāhuku increase turbulent transport of cloud droplets through vertical space. The small sample size may be another limitation to our CWI model because the model was fitted to only five data points (locations). Field measurements at additional locations with various vegetation structures would help us to evaluate the applicability of the model more broadly.

While we originally proposed to measure LWC using a commercial LWC sensor, the proposed instrument was later found to be unsuitable for long-term monitoring in the field as most commercial LWC sensors are designed to be used on aircraft. A visibility sensor was tested as an alternative LWC sensor, but technical problems and large uncertainties due to the nonlinear relationship between visibility and LWC were found during preliminary analyses. Therefore, we selected the Juvik fog gauge as the primary sensor to monitor LWC. Two additional experiments had to be conducted for the calibration of the fog gauge. Raindrop characteristics were required for correcting wind-driven rain errors in the Juvik gauge. Because there were no recent studies on ground-based raindrop measurements in Hawaiʻi, we used a laser disdrometer to test models of raindrop DSD and terminal velocity. Although the disdrometer data matched the MP model reasonably well, additional field measurements to collect higher precision disdrometer data is needed to improve the Juvik gauge error correction method. To calculate the Juvik fog gauge efficiency, we collaborated with the UH Manoa Atmospheric Sciences Department to design a mobile station to collect LWC data under field conditions. Additional data collection under different environmental conditions is needed to improve model estimates.

We were unable to complete the testing of regional climate model simulations of CWF because the model simulation output was not in a format readily available for our analyses. We also collected time-lapse camera imagery during the study, although it has not been analysed and may require a machine learning approach. We will continue to pursue these objectives.

Sapflux measurements revealed a strong relationship between tree transpiration and VPD in native koa trees at the Nakula field site. Conditions at the leaf surface were highly coupled to the atmosphere; fog decreased atmospheric and leaf surface VPD. Fog, which occurred mainly during the day at the Nakula site, also decreased solar radiation. Without fog, transpiration would be higher due to the effects of both higher VPD from lower air humidity and higher stomatal conductance due to higher light levels. Trees at the Nakula site exhibited relatively high rates of nighttime sapflux, accounting for more than 35% of total daily transpiration. Because fog does not frequently occur at night, fog effects on nighttime transpiration were modest.

Further analysis of this rich sensor dataset could examine specific events of fog immersion and rainfall and their influences on moisture at different soil depths during the dry season to determine whether they produce an observable effect on plant water relations and growth. Integration of the high frequency dendrometer data with sapflow data seems a natural next step, since the observation of sapflux suggests that daytime fog immersion suppresses VPD and may support higher daytime plant growth, even if the fog does not contribute directly to soil moisture.

Very little difference in soil moisture was detected between grass control and treatment plots at 5 cm depth, and none at the deeper, 20 cm depth. This suggests that grass removal for restoration activities does reduce cloud water interception and, hence, does not necessarily reduce soil moisture availability that could impact native plant recruitment, even in exposed areas such as Nakula. Seedling survival rates documented during this study, considered with previous work conducted by Warren et al. (2019), suggest that fog may play a buffering role from the effects of intense solar radiation. Other converted TMCF landscapes may benefit from a similar grass-removal restoration approach.

ix. OUTREACH:

Public Outreach

Fortini, L. (2018). Applied landscape ecology for changing Pacific Islands. Meeting between Pacific Island USGS scientists and FWS management partners, 20 March 20, 2018.

Fortini, L. (2019). Overview of climate-related research relevant to plant conservation in Hawaii. Presented at the Army Natural Resources Program of Oahu annual meeting, 5 August, 2019.

Giambelluca, T. (2020). ʻIke Wai – Water Resources Research Center Stakeholder Workshop, 20 February, 2020.

Publications and Conference Presentations

Mair, A., Kāne, H., Johnson, A.G., Rotzoll, K. and Oki, D.S., 2020, Water-budget modeling to evaluate effects of climate change and drought on groundwater recharge and wildfire risk, State of Hawaiʻi: Water Resources Research Center Webinar, University of Hawaiʻi at Mānoa, December 9.

Tseng, H., Giambelluca, T. W., DeLay, J. K., and Nullet, M. A. (2017). *Cloud water interception and canopy water balance in the Hawaiian Islands: preliminary results and emerging patterns.* Paper presented at the AGU Fall Meeting.

Berio Fortini, L. (2018). Using dendrometers to help the conservation of extremely rare plants in Hawaii. Hawaii Conservation Conference, 24 July 2018.

Tseng, H., Giambelluca, T. W., Small Griswold, J. D., Freitag, S., Howell, S. G., Nugent, A., . . . DeLay, J. K. (2018). *Testing alternative ground-based cloud liquid water content measurement methods for estimating cloud water interception in tropical montane cloud forests.* Paper presented at the AGU Fall Meeting.

Kennedy, J.J., Mair, A., Perkins, K.S., Nullet, M.A., Tseng, H., and Miyazawa, Y. (2019). Summary of soil field-saturated hydraulic conductivity, hydrophobicity, and preferential-flow measurements and soil laboratory-testing results collected at three sites on the islands of Maui and Hawaii, Hawaii, July 2016–January 2018: U.S. Geological Survey data release, https://doi.org/10.5066/P9J5SESD

Tseng, H., Giambelluca, T., and DeLay, J. (2019). *Cloud Water Interception in Hawaiʻi: Project Overview* Mair, A., and Giambelluca, T., 2019, Quantifying impacts of high-priority non-native forest species on freshwater availability in the State of Hawaiʻi — proposed next steps: Stakeholder Meeting, State of Hawaiʻi Commission on Water Resource Management, Honolulu, June 17.

Mair, A., and Giambelluca, T., 2019, Impacts of non-native forest species on freshwater availability — implications for watershed management and restoration, U.S. Geological

Survey Pacific Islands Water and Ecosystems Science Meeting, University of Hawaiʻi at Mānoa, Honolulu, September 18.

Mair, A., Berio Fortini, L., and Giambelluca, T., 2019, Impacts of non-native forest species on freshwater resources in the State of Hawaiʻi — proposed next steps: Stakeholder Webinar, November 1.

Tseng, H., Giambelluca, T., DeLay, J., and Nullet, M. (2019). *Cloud water interception in Hawaiʻi: project overview and preliminary results of fog and CWI patterns.* Paper presented at the 8th International Conference on Fog, Fog Collection and Dew.

Mair, A., 2020, Quantifying the impacts of land-cover change and climate variability on freshwater resources in the State of Hawaiʻi: Pacific Climate and Invasive Species Working Group Webinar, July 1.

Mair, A., Rotzoll, K., and Izuka, S., 2020, Application of water-budget models to evaluate the effects of forest change on water resources in Hawaiʻi — information needs to reduce model uncertainty: Hawaiʻi Conservation Conference, September 1.

Tseng, H., Giambelluca, T., Griswold, J., Freitag, S., Howell, S., Nugent, A., . . . Nullet, M. (2019). *Fog gauge measurements of cloud liquid water content: proposing a new standard.* Paper presented at the 8th International Conference on Fog, Fog Collection and Dew.

Tseng, H., Giambelluca, T. W., and Nullet, M. (2020). *Cloud water interception by different types of montane vegetation in Hawai ʻi.* Paper presented at the AGU Fall Meeting.

Planned Publications and Presentations

Berio Fortini, L., Kagawa-Viviani, A., Yelenik, S., Tseng, H., Giambelluca, T. In preparation. Assessing the role of cloud water and other environmental factors in native plant growth and recruitment at a high-elevation restoration site in Maui, Hawaii.

Berio Fortini, L., Kagawa-Viviani, A., Yelenik, S., Tseng, H., Giambelluca, T. (2022). Assessing the role of cloud water and other environmental factors in native plant growth and recruitment at a high-elevation restoration site in Maui, Hawaii. Hawaii Conservation Conference.

Tseng, H., & Giambelluca, T. (2021). Cloud Water Interception in Hawai'i: Climate vs Vegetation Influences*.* Paper to be presented at the International Tropical Islands Water Conference, April 12, 2021.

Tseng, H., & Giambelluca, T. (In preparation). Cloud water interception in Hawaiʻi: III. Predicting cloud water interception by horizontal cloud water flux and canopy structure.

Tseng, H., Giambelluca, T., & Nullet, M. (In preparation). Cloud water interception in Hawaiʻi: II. The impact canopy water balance model temporal resolution on estimates of cloud water interception.

Tseng, H., Giambelluca, T., Griswold, J., Nanko, K., Freitag, S., Howell, S., . . . Nullet, M. (In preparation). Cloud water interception in Hawaiʻi: I. Calibration of passive fog gauge as an low-cost liquid water content sensor for remote tropical montane cloud forest sites.

ACKNOWLEDGMENTS

We thank the National Area Reserve System for enabling our work at the Kaʻala field site. The Park HQ and Nāhuku field sites were within Haleakalā National Park (HALE) and Hawaiʻi Volcanoes National Park (HAVO), respectively. We are grateful to the National Park Service staff, especially Woody Malinson (HALE) and Rhonda Loh (HAVO) for facilitating our research in the parks. The work at the Nakula field site was completed with the help of several personnel from the Maui Forest Bird Recovery Team, including: Eli Rose, Christopher Warren, Hanna Mounce, Eric Preston Hamren, Laura Berthold and the whole MFBR team. We are grateful for access to the Laupāhoehoe field site within the Hawaiʻi Experimental Tropical Forest, and the climate tower operated and maintained by the US Forest Service, Institute for Pacific Islands Forestry.

REFERENCES

Alvarado-Barrientos, M. S., F. Holwerda, H. Asbjornsen, T. E. Dawson, and L. A. Bruijnzeel. 2014. Suppression of transpiration due to cloud immersion in a seasonally dry Mexican weeping pine plantation. *Agricultural and Forest Meteorology* 186:12–25.

Atlas, D., Srivastava, R.C., and Sekhon, R.S. (1973). Doppler radar characteristics of precipitation at vertical incidence. *Reviews of Geophysics, 11*(1), 1-35. doi: 10.1029/RG011i001p00001.

Baguskas, S.A., Still, C.J., Fischer, D.T., D'Antonio, C.M., King, J.Y. (2016). Coastal fog during summer drought improves the water status of sapling trees more than adult trees in a California pine forest. *Oecologia 181(1)*,137-148. doi: 10.1007/s00442-016-3556-y.

Barton, K. (2020). MuMIn: Multi-Model Inference. R package version 1.43.17. https://CRAN.R-project.org/package=MuMIn.

Bittencourt, P.R.L., Barros, F. de V., Eller, C.B., Müller, C.S., and Oliveira, R.S. (2019). The fog regime in a tropical montane cloud forest in Brazil and its effects on water, light and microclimate. *Agricultural and Forest Meteorology* 265:359–369.

Blanchard, D.C. (1953). Raindrop size-distribution in hawaiian rains. *Journal of Meteorology, 10*(6), 457-473. doi: 10.1175/1520-0469(1953)010<0457:rsdihr>2.0.co;2.

Bräuning, A., Volland-Voigt, F., Burchardt, I., Ganzhi, O., Nauss, T., and Peters, T. (2009). Climatic Control of Radial Growth of *Cedrela montana* in a Humid Mountain Rainforest in Southern Ecuador. *Erdkunde* 63:337–345.

Brauman, K.A., Freyberg, D.L., Daily, G.C. (2010). Forest structure influences on rainfall partitioning and cloud interception: A comparison of native forest sites in Kona, Hawai'i.

Agricultural and Forest Meteorology 150(2), 265-275. doi: https://doi.org/10.1016/j.agrformet.2009.11.011.

Burgess, S.S., Adams, M.A., Turner, N.C., Beverly, C.R., Ong, C.K., Khan, A.A., and Bleby, T.M. (2001). An improved heat pulse method to measure low and reverse rates of sap flow in woody plants. *Tree Physiology, 21*(9), 589-598.

Burnham, K.P., Anderson, D.R. (2002). Model Selection and Inference: a Practical Information-theoretic Approach. 2d. ed. New York: Springer:Vertag.

Carbone, M.S., Williams, A.P. Ambrose, A.R., Boot, C.M., Bradley, E.S., Dawson, T.E., Schaeffer, S.M., Schimel, J.P., Still, C.J. (2012). Cloud shading and fog drip influence the metabolism of a coastal pine ecosystem. Global Change Biology 19(2), 484-497. doi: https://doi.org/10.1111/gcb.12054.

Choat, B., Jansen, S., Brodribb, T.J., Cochard, H., Delzon, S., Bhaskar, R., . . . Zanne, A. E. (2012). Global convergence in the vulnerability of forests to drought. *Nature, 491*(7426), 752-755. doi: 10.1038/nature11688

Chuang, P.Y., Saw, E.W., Small, J.D., Shaw, R.A., Sipperley, C.M., Payne, G.A., and Bachalo, W.D. (2008). Airborne Phase Doppler Interferometry for Cloud Microphysical Measurements. *Aerosol Science and Technology, 42*(8), 685-703. doi: 10.1080/02786820802232956

Copeland, S.M., Munson, S.M., Bradford, J.B., Butterfield, B.J. and Gunnell, K.L. (2019). Long-term plant community trajectories suggest divergent responses of native and non-native perennials and annuals to vegetation removal and seeding treatments. *Restoration Ecology*, *27*(4), pp.821-831.

Corbin, J.D., Thomsen, M.A., Dawson, T.E. et al. (2005) Summer water use by California coastal prairie grasses: fog, drought, and community composition. *Oecologia* 145, 511–521.

Dang, Q.-L., Margolis, H.A., and Collatz, G.J. (1998). Parameterization and testing of a coupled photosynthesis–stomatal conductance model for boreal trees. *Tree Physiology, 18*(3), 141-153. doi: 10.1093/treephys/18.3.141

Dawson T.E. (1998). Fog in the California redwood forest: ecosystem inputs and use by plants. *Oecologia* 117:476–485

DeLay, J. K., & Giambelluca, T. W. (2011). 35 History of fog and cloud water interception research in Hawai'i. Tropical Montane Cloud Forests: Science for Conservation and Management, 332-358.

Ehrenberger, W., Rüger, S., Fitzke, R., Vollenweider, P., Günthardt-Georg, M., Kuster, T., Zimmermann, U., Arend, M. (2012). Concomitant dendrometer and leaf patch pressure probe measurements reveal the effect of microclimate and soil moisture on diurnal stem water and leaf turgor variations in young oak trees. *Functional Plant Biology 39(4)*, 297–305.

Eller, C.B., Lima, A.L., and Oliveira, R.S. (2013). Foliar uptake of fog water and transport belowground alleviates drought effects in the cloud forest tree species, Drimys brasiliensis (Winteraceae). *New Phytologist* 199:151–162.

Estrela, M.J., Valiente, J.A., Corell, D., Fuentes, D. and Valdecantos, A. (2009). Prospective use of collected fog water in the restoration of degraded burned areas under dry Mediterranean conditions. *Agricultural and forest meteorology*, *149*(11), pp.1896-1906.

Fischer D.T., C.J. Still, and A.P. Williams (2009). Significance of summer fog and overcast for drought stress and ecological functioning of coastal CA endemic plant species. *Journal of Biogeography*, 36:783–799.

Fox, J. and Weisberg, S. (2019). An R Companion to Applied Regression, Third Edition. Thousand Oaks CA: Sage. URL: https://socialsciences.mcmaster.ca/jfox/Books/Companion/

Giambelluca, T.W., and Gerold, G. 2011. Hydrology and biogeochemistry of tropical montane cloud forests. Chapter 11 in D.F. Levia, D.E. Carlyle-Moses, and T. Tanaka (eds.), *Forest Hydrology and Biogeochemistry: Synthesis of Research and Future Directions*. Ecological Studies Series, No. 216, Springer-Verlag, Heidelberg, Germany.

Giambelluca, T.W., DeLay, J.K., Nullet, M.A., Scholl, M., and Gingerich, S.B. (2011a). Interpreting canopy water balance and fog screen observations: separating cloud water from wind-blown rainfall at two contrasting forest sites in Hawai'i. In F. N. Scatena, L. A. Bruijnzeel and L. S. Hamilton (Eds.), *Tropical Montane Cloud Forests: Science for Conservation and Management* (pp. 342-351). Cambridge: Cambridge University Press.

Giambelluca, T.W., Shuai, X., Barnes, M.L., Alliss, R.J., Longman, R.J., Miura, T., . . . Businger, A.D. (2014). Evapotranspiration of Hawai‘i - Final Report: U.S. Army Corps of Engineers – Honolulu District, Commission on Water Resource Management, State of Hawai‘i.

Gotsch, S.G., Crausbay, S.D., Giambelluca, T.W., Weintraub, A.E., Longman, R.J., Asbjornsen, H., . . . Dawson, T.E. (2014). Water relations and microclimate around the upper limit of a cloud forest in Maui, Hawai‘i. *Tree Physiology, 34*(7), 766-777. doi: 10.1093/treephys/tpu050

Hansen, E., and Juvik, J.O. (2010). Performance of a Louvered Screen Fog Gauge as a Proxy for Canopy Throughfall in a Hawaiian Montane Cloud Forest. *Pacific Agriculture and Natural Resources, 2*, 26-30.

Jarvis, P.G., and McNaughton, K.G. (1986). Stomatal control of transpiration: scaling up from leaf to region. *Advances in ecological research, 15*, 1-49.

Juvik, J.O., and Nullet, D. (1995). Relationships Between Rainfall, Cloud-Water Interception, and Canopy Throughfall in a Hawaiian Montane Forest. In L. S. Hamilton, J. O. Juvik and F. N. Scatena (Eds.), *Tropical Montane Cloud Forests* (pp. 165-182). New York, NY: Springer US.

Katata, G., Nagai, H., Wrzesinsky, T., Klemm, O., Eugster, W., and Burkard, R. (2008). Development of a Land Surface Model Including Cloud Water Deposition on Vegetation. *Journal of Applied Meteorology and Climatology, 47*(8), 2129-2146. doi: 10.1175/2008jamc1758.1

Katata, G., Kagino, M., Hiraki, T., Aikawa, M., Kobayashi, T., Nagai, H. (2011). A method for simple and accurate estimation of fog deposition in a mountain forest using a meteorological model. *Journal of Geophysical Research 116(D20)*, D20102. doi: https://doi.org/10.1029/2010JD015552.

Kennedy, J.J., Mair, A., Perkins, K.S., Nullet, M.A., Tseng, H., and Miyazawa, Y. (2019). Summary of soil field-saturated hydraulic conductivity, hydrophobicity, and preferential-flow measurements and soil laboratory-testing results collected at three sites on the islands of Maui and Hawaii, Hawaii, July 2016–January 2018: U.S. Geological Survey data release, https://doi.org/10.5066/P9J5SESD.

Köcher, P., Horna, V., and Leuschner, C. (2012). Environmental control of daily stem growth patterns in five temperate broad-leaved tree species. *Tree Physiology* 32:1021–1032.

Kulmatiski, A., Beard, K.H., Verweij, R. J. T., Edmund C. (2010). A depth-controlled tracer technique measures vertical, horizontal and temporal patterns of water use by trees and grasses in a subtropical savanna. *New Phytologist 188(1)*, 199-209. doi: https://doi.org/10.1111/j.1469-8137.2010.03338.x.

Kulmatiski, A., Beard, K.H. (2013). Root niche partitioning among grasses, saplings, and trees measured using a tracer technique. *Oecologia 171*, 25-37. doi: 10.1007/s00442-012-2390-0.

Levine, J.M., McEachern, A.K. and Cowan, C. (2008). Rainfall effects on rare annual plants. *Journal of Ecology*, 96(4), pp.795-806.

MacNally, R. and Walsh, C.J. (2004). Hierarchical partitioning public-domain software. *Biodiversity and Conservation*, 13, 659-660. https://search.proquest.com/openview/6f19c4d612b6cf75b106c479e7084a58/1.

Marshall, J.S., and Palmer, W.M.K. (1948). The distribution of raindrops with size. *Journal of Meteorology, 5*(4), 165-166. doi: 10.1175/1520-0469(1948)005<0165:tdorws>2.0.co;2

Monteith, J.L. (1965). Evaporation and environment Symposia of the Society for Experimental Biology (Vol. 19, pp. 205–224): Cambridge University Press (CUP) Cambridge.

Nanko, K., Hotta, N., and Suzuki, M. (2006). Evaluating the influence of canopy species and meteorological factors on throughfall drop size distribution. *Journal of Hydrology, 329*(3), 422-431. doi: https://doi.org/10.1016/j.jhydrol.2006.02.036

Oberhuber, W., Kofler, W., Schuster, R.... (2015). Environmental effects on stem water deficit in co-occurring conifers exposed to soil dryness. *International Journal of Biometeorology 59*, 417–426. doi: https://doi.org/10.1007/s00484-014-0853-1.

Ostertag, R., Inman-Narahari, F., Cordell, S., Giardina, C.P., and Sack, L. (2014). Forest Structure in Low-Diversity Tropical Forests: A Study of Hawaiian Wet and Dry Forests. *PLOS ONE, 9*(8), e103268. doi: 10.1371/journal.pone.0103268

Peterson, R.A. (2019). Ordered quantile normalization: a semiparametric transformation built for the cross-validation era. *Journal of Applied Statistics*, 1-16.

Phillips, N., and Oren, R. (1998). A comparison of daily representations of canopy conductance based on two conditional time-averaging methods and the dependence of daily conductance on environmental factors. *Annales Des Sciences Forestieres, 55*(1-2), 217-235.

R Core Team (2020). R: A language and environment for statistical computing. R Foundation for Statistical Computing, Vienna, Austria. URL https://www.R-project.org/.

Scholl, M.A., Giambelluca, T.W., Gingerich, S.B., Nullet, M.A., and L.L. Loope. (2007). Cloud water in windward and leeward mountain forests: The stable isotope signature of orographic cloud water. *Water Resources Research* 43:W12411.

Spannl, S., Volland, F., Pucha, D., Peters, T., Cueva, E., and Bräuning, A. (2016). Climate variability, tree increment patterns and ENSO-related carbon sequestration reduction of the tropical dry forest species *Loxopterygium huasango* of Southern Ecuador. *Trees* 30:1245–1258.

Stanton, D.E., Armesto, J.J. and Hedin, L.O. (2014). Ecosystem properties self-organize in response to a directional fog–vegetation interaction. *Ecology*, 95(5), pp.1203-1212.

Takahashi, M., Giambelluca, T.W., Mudd, R.G., DeLay, J.K., Nullet, M.A., and Asner, G.P. (2011). Rainfall partitioning and cloud water interception in native forest and invaded forest in Hawai'i Volcanoes National Park. *Hydrological Processes, 25*(3), 448-464. doi: 10.1002/hyp.7797

Vieira, D.L. and Scariot, A. (2006). Principles of natural regeneration of tropical dry forests for restoration. *Restoration Ecology*, 14(1), pp.11-20.

Wainwright, C.E., Wolkovich, E.M., and Cleland, E.E. (2012). Seasonal priority effects: implications for invasion and restoration in a semi-arid system. *Journal of Applied Ecology*, 49(1), pp.234-241.

Warren, C.C., Mounce, H.L., Berthold, L.K., Farmer, C., Leonard, D., Duvall, F. (2019). Experimental restoration trials in Nakula Natural Area Reserve in preparation for reintroduction of Kiwikiu (Pseudonestor xanthophrys). Pacific Cooperative Studies Unit Technical Report #199. University of Hawai‘i at Mānoa, Department of Botany. Honolulu, HI. 102 pages.

Yelenik, S.G. and Levine, J.M. (2010). Processes limiting native shrub recovery in exotic grasslands after non-native herbivore removal. *Restoration Ecology*, 18, pp.418-425.

Ziaco, E., Biondi, F. (2018). Stem Circadian Phenology of Four Pine Species in Naturally Contrasting Climates from Sky-Island Forests of the Western USA. Forests 9(7), 396. doi: https://doi.org/10.3390/f9070396.

Zweifel, R., Zimmerman, L., Newbery D.M. (2005). Modeling tree water deficit from microclimate: an approach to quantifying drought stress. Tree Physiology 25(2), 147-156. doi: https://doi.org/10.1093/treephys/25.2.147https://doi.org/10.1093/treephys/25.2.147.